LBL-11970
Preprint

Lawrence Berkeley Laboratory
UNIVERSITY OF CALIFORNIA

Materials & Molecular
Research Division

Submitted to the Journal of Chemical Physics

INFRARED VIBRATIONAL PREDISSOCIATION SPECTROSCOPY OF WATER CLUSTERS BY THE CROSSED LASER - MOLECULAR BEAM TECHNIQUE

M.F. Vernon, D.J. Krajnovich, H.S. Kwok,
J.M. Lisy, Y.R. Shen, and Y.T. Lee

November 1981

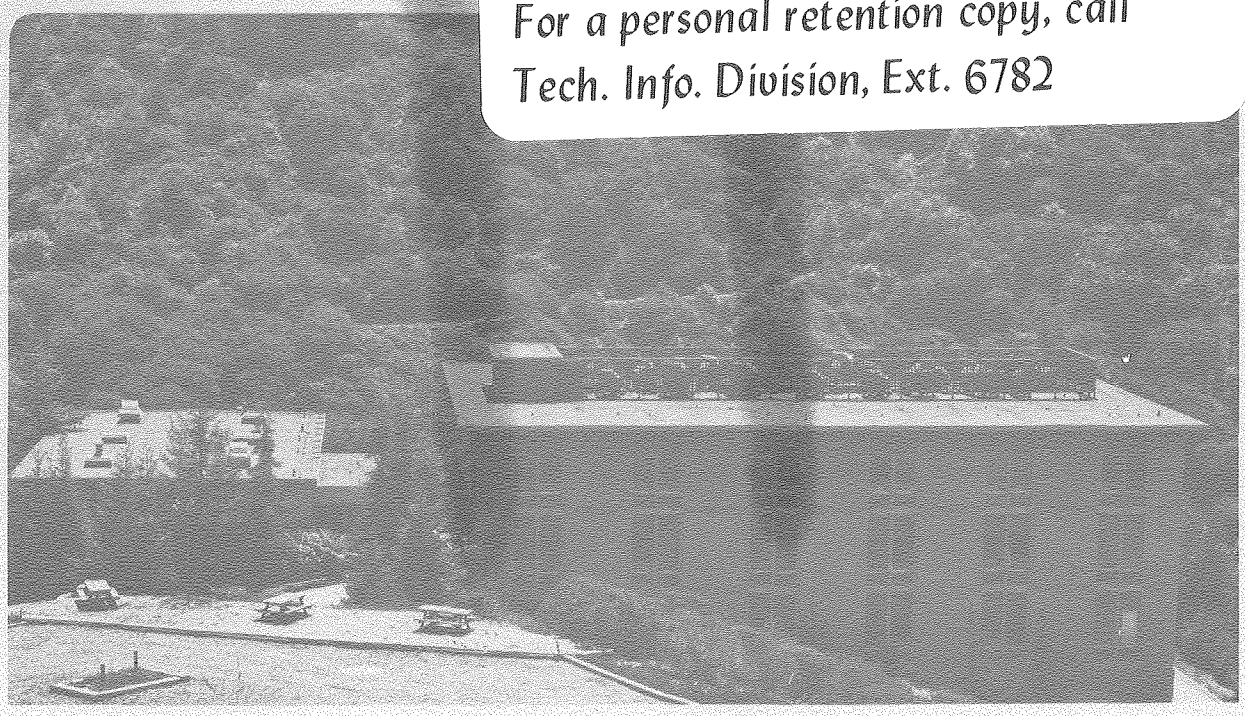

Prepared for the U.S. Department of Energy under Contract W-7405-ENG-48

DISCLAIMER

INFRARED VIBRATIONAL PREDISSOCIATION SPECTROSCOPY OF WATER CLUSTERS BY THE CROSSED LASER - MOLECULAR BEAM TECHNIQUE*

M. F. Vernon, D. J. Krajnovich, H. S. Kwok,
J. M. Lisy,+ Y. R. Shen and Y. T. Lee

Lawrence Berkeley Laboratory
Department of Chemistry
University of California
Berkeley, California 94720

Abstract

Water clusters formed in a molecular beam are predissociated by tunable, pulsed, infrared radiation in the frequency range 2900-3750 cm^{-1}. The recoiling fragments are detected off axis from the molecular beam using a rotatable mass spectrometer. Arguments are presented which show that the measured frequency dependent signal at a fixed detector angle is proportional to the absorption spectrum of the clusters. It is found that the spectra of clusters containing three or more water molecules are remarkably similar to the liquid phase spectrum.

Dynamical information on the predissociation process is obtained from the velocity distribution of the fragments. An upper limit to the excited vibrational state lifetime of ~1 microsecond is observed

---

*This work was supported by the Director, Office of Energy Research, Office of Basic Energy Sciences, Chemical Sciences Division of the U.S. Department of Energy under Contract No. W-7405-ENG-48 and the Assistant Secretary for Nuclear Energy, Office of Advanced Systems and Nuclear Projects, Advanced Isotope Separation Division, U. S. Department of Energy under Contract No. W-7405-Eng-48.

+National Science Foundation Postdoctoral Fellow 1979-1980.

for the results reported here. The most probable dissociation process concentrates the available excess energy into the internal motions of the fragment molecules. Both the time scale and translational energy distribution are consistent with the qualitative predictions of current theoretical models for cluster predissociation. From adiabatic dissociation trajectories and Monte Carlo simulations it is seen that the strong coupling present in the water polymers probably invalidates the simpler "diatomic" picture formulations of cluster predissociation. Instead, the energy can be extensively shared among the intermolecular motions in the polymer before dissociation.

Comparison between current intermolecular potentials describing liquid water and the observed frequencies is made in the normal mode approximation. The inability of any potential to predict the gross spectral features (the number of bands and their observed frequency shift from the gas phase monomer) suggests that substantial improvement in the potential energy functions are possible, but that more accurate methods of solving the vibrational wave equation are necessary before a proper explanation of the spectral fine structure is possible.

The observed differences between the dimer and larger polymers (trimer-hexamer) indicate a dramatic change in the hydrogen bonding, which is best explained as arising from the non-additive effects present when a water molecule is both donating and accepting a hydrogen bond. This difference between dimer and trimer also rationalizes the previous disagreement between potential functions based on condensed

phase properties (where the water molecule is interacting with multiple neighbors) and those fit to imperfect gas or dimer properties which sample only the isolated pair potential. The data support an interpretation of the hydrogen bonded O-H stretching fundamental region as arising from a homogeneous broadening (not necessarily a result of the predissociation) whose width is characterstic of the hydrogen bond itself and not the sum of distinct bonding geometries. This is different from some previous theories of the water infrared absorption spectrum which assign each band to water molecules bound to different numbers of neighboring molecules.

Introduction

An outstanding problem of chemical physics is understanding the structure and dynamics of condensed phases. Substantial agreement between theory and experiment has been made for the weakly interacting rare gases where, as Barker et. al.[1] have shown, a single realistic pair interaction potential has been able to accurately fit experimental data of all phases due to the domination of pairwise additive potentials in these systems. Conversely, for strongly interacting molecules such as water, no single pair potential has yet been proposed which accurately reproduces the known physical properties of this substance in all phases.[2] The strong orientational forces responsible for hydrogen bonding are notoriously difficult to theoretically model.

In 1951 Rowlinson[3] proposed the first molecular model aimed at a quantitative prediction of solid state properties, beginning with known gas phase properties. The model represented the water monomers by a four point tetrahedral charge distribution which reproduced the gas phase dipole moment. An orientation-independent Lennard-Jones potential was adjusted to fit the second virial coefficient and represented the short-range overlap repulsion and long-range dispersion interactions between pairs of water molecules. Satisfactory agreement with the lattice spacing and lattice energy of ice were obtained with this model.

Subsequently, many different pair potentials have been published. The Ben-Naim Stillinger potential,[4a,b] for example, was an "effective"

pair potential for the liquid which partially accounted for many-body effects. An extensive series of ab initio calculations have also been performed by Clementi and co-workers.[5a-g] Beginning with Hartree-Fock potentials for the water dimer, studies were made of the effects of configuration interaction, empirical dispersion terms, and many-body effects on the structure of the liquid and small polymers predicted by these pairwise additive potentials. The conclusions of these ab initio studies were that the liquid state structural properties were predicted as well as by any other current potential, that the three body interaction accounts for approximately 10 percent of the binding energy and has no strong angular dependence, and that analytical fits to Hartree-Fock calculations, suitably corrected for the dispersion interaction, can reproduce results in an economical form.

Current trends in theory are toward a quantitatively accurate model of water suitable for studying solution behavior and water interactions with proteins.[6] The suitability criterion implies that the model must be computationally economical, such as a central force model. The experimental properties which are currently used to compare potentials fall into two groups. The first group consists of liquid state structural properties, such as the radial distribution functions determined from x-ray and neutron diffraction experiments. The second group consists of isolated pair interaction properties, such as second virial coefficients and the structural parameters of the gas phase dimer. When potentials

which have been designed to predict one of these groups of properties are used to calculate the others, agreement has not been very satisfactory. Although it has been suggested that the limitations of the central force model itself might be the source of disagreement,[2] there is no direct evidence to believe that a suitable central force pair potential cannot be found which satisfactorly reproduces the available experimental data.

The determination of the potential parameters is difficult because the available experimental data are largely integral quantities which depend on many different regions of the potential surface. Consequently, errors in the repulsive interaction can be compensated by errors in the attractive well so that a single experimental observable can always be fit. Moreover, even when disagreement is observed in other properties, it is not clear which region of the potential is responsible, and a trial and error method of adjusting the potential parameters has been the method of choice in improving agreement with experimental data. To better discriminate against potential forms, microscopic data sensitive to well defined regions of the potential energy surface are needed.

An approach which has been successful recently in determining condensed phase properties is the study of the change in the properties of small clusters of molecules as the cluster size increases. Ideally, information is obtained on the rate at which clusters approach bulk phase behavior for a particular observable. Examples of such an approach include the relation between the photoionization thresholds of alkali

metal clusters and the work function of the bulk metal, and the laser induced fluorescence (LIF) spectra of I_2-(rare gas)$_n$ clusters,[8] where binding energies and propensity rules for the predissociation product states were obtained as a function of the cluster size, n. Most recently, resonant two photon ionization spectroscopy[65] and ultraviolet fluorescence excitation spectra[66] of benzene clusters have investigated the approach to the electronic bands of condensed phase benzene.

Analogous infrared spectral trends in the clusters of water have been experimentally available since the original matrix isolation work of Pimentel and co-workers.[9] In these studies, the dependence of infrared absorption linestrengths on the matrix to absorber ratio was used to assign the various absorption bands to specific polymers. The problems of overlapping absorptions bands limited the application of the matrix isolation technique to principally the dimer and trimer. No similarity with the broad, structureless infrared spectrum of liquid water was observed. More recently, Luck[10] has carefully followed the concentration dependence of the infrared matrix absorptions to extend the correlations between bands and polymer sizes. This information has not been compared to current potentials.

The infrared and Raman spectra of water and ice, although extensively studied in the laboratory,[11] have not figured prominently in the analysis of potential forms, due to an uncertainty in the assignment of the observed features and the difficulty of computing infrared spectra in condensed phases.

Recent studies by Sceats, Rice, and co-workers on amorphous ice[12] have provided additional insight into the role of disorder in complicating the Raman and infrared spectra of condensed phases of water. A detailed random network model (RNM) was developed to calculate the required spectral properties.[13] A wide range of experimental data was used to model the intermolecular and intramolecular potentials of hydrogen bonded water, and the agreement with the observations on amorphous ice using the RNM was good. Additionally, Morse and Rice[14] have begun comparing the properties of different ice phases with intermolecular potentials, showing that the predicted crystal structures from various potential models vary dramatically.

An additional property sensitive to features of the interaction potential of water clusters is the time scale for predissociation of vibrationally excited clusters containing energy in excess of the hydrogen bond energy. Vibrational predissociation of clusters has been reported by many researchers using a variety of lasers and detection techniques.[15] The focus of this previous work has been toward measuring the shifts of the monomer absorption features which occur in the complexes. Except for the detailed study of the I_2--rare gas series by Levy et al., little is known about the energy disposal mechanisms and dissociation rates of these unstable clusters.

In 1933, Stepanov[16] proposed that the broadening of the hydrogen bonded infrared vibrational spectra might be a result of predissociation. More recently, Hagen and Kassner[17] have calculated the decay rate for water trimers as a function of temperature based on a Slater

type model. Robertson/Coulson,[18a-c] Ewing,[19] and Beswick/Jortner[20] have all calculated predissociation rates for binary complexes using first order time dependent perturbation theory. This current theoretical work has shown that the dissociation rate is intimately connected with the mode of energy disposal. From the Ewing and Beswick/Jortner models of vibrational predissociation in binary clusters, the dominating factor is the amount of energy placed in relative translational motion of the dissociation fragments. The dissociation rate is governed by the poor overlap between the continuum translational wavefunction and the vibrationally excited "bound" state of the complex. The small Frank-Condon factor produces slow dissociation rates for predissociations with large amounts of translational energy, predicting that any channels which reduce the product kinetic energy are favored, and that the fragments from such channels will be vibrationally or rotationally excited from energy conservation.

Experimental studies on relaxation lifetimes in liquid H_2O have included dielectric,[21] nuclear quadrupole resonance,[22] inelastic neutron scattering,[23] and depolarized Rayleigh scattering (DPRS).[24] The 2-5 picosecond relaxation times observed in the room temperature dielectric and NQR studies have been related to orientational lifetimes in liquid water. The DPRS experiments measure two lifetimes. The slower component is similar to the reorientational time scale of the NQR and neutron scattering results, while the fast component of 0.6 picoseconds has an Arrhenius temperature dependence with a 3 kcal/mole activation energy. This fast lifetime was interpreted as the time

constant for breaking a hydrogen bond, with the activation energy measuring the energy difference between waters oriented in the proper direction for hydrogen bonding and those that are not. The induction period for the other relaxation processes which depend on reorientation suggests that the breaking of a hydrogen bond is the rate determining step before reorientation can occur. The vibrational predissociation lifetimes would then be expected to be longer than 1 picosecond, depending also on the hydrogen bond breaking rate.

With this background, the current work was undertaken to provide infrared spectra of selected polymers in order to assign the features in the vibrational spectra and relate these assignments to current water potentials. Using the crossed laser-molecular beam technique, the frequency dependence of the predissociation fragment yield is measured, enabling improved spectroscopic assignments to be made as a result of the mass selective detection scheme. Additional measurements of the velocity distributions of the predissociation fragments give directly the translational energy released in the predissociation. From these new observations, an explanation for the discrepancy between the condensed phase water and gas phase pair interactions is given. The infrared spectra are seen to be quite sensitive to the proposed intermolecular potential model and should figure prominently in determining future intermolecular water potentials.

Experimental

The general features of the molecular beam apparatus have been discussed elsewhere.[25a-c] Briefly, a molecular beam of water containing a small percentage of water clusters was crossed at right angles by pulsed, tunable infrared radiation inside a liquid nitrogen cooled interaction chamber. The absorption of light by water clusters in the frequency range probed is sufficient to cause vibrational predissociation. The predissociation products were detected in the plane of the molecular and infrared beams by a rotatable, ultra-high vacuum mass spectrometer consisting of an electron bombardment ionizer, quadrupole mass filter, and particle counter.

The molecular beam source and differential pumping scheme were modified as shown in Fig. 1 to define the beam to approximately 1.5^{o} FWHM and eliminate any direct view by the detector of the differential pumping regions. The molecular beam was formed by expanding neat water vapor through a heated 0.18 mm diameter nozzle held at $125^{o}C$. To vary the cluster distribution, the backing pressure was adjusted by controlling the temperature of the water reservoir. Expansion with He as a carrier gas was attempted hoping to reduce the molecular beam velocity dispersion, but the dilution necessary to control the condensation gave too little signal to be practical.

The tunable infrared radiation (2900-6500 cm^{-1}) was produced by passing the output from a pulsed Nd:YAG laser (Quanta Ray Model DCR) operating at 10 Hz into a temperature stabilized $LiNbO_3$ crystal contained in the L-shaped cavity shown in Fig. 2. The optical

parametric oscillation (OPO) process which produces the infrared radiation has been well studied.[26] The OPO linewidth was determined by measuring the frequencies at the half power points as a function of monochromator slit size and extrapolating to zero slit width. The linewidth varied from 4 cm^{-1} to 10 cm^{-1} as the idler frequency was scanned from 3000 to 4000 cm^{-1}. These values are in accord with those expected for a single pass oscillator within the accuracy of the experimental technique. The energy in the frequency range 3000-4000 cm^{-1} was typically 1-4 millijoules per pulse with 1 joule/cm^2 of Nd:YAG pump energy fluence. The laser pulse duration is less than 10 nanoseconds, and linearly polarized perpendicular to the rotating plane of the detector.

Because there is always a distribution of polymer species in the molecular beam, and because unique identification of the water clusters in the electron bombardment ionizer is not possible, we wish to emphasize that we are unable to directly measure the vibrational predissociation spectrum of $(H_2O)_n$ with a prescribed n. However, one important feature of the mass selective detection scheme is that it acts as a "high-pass" filter; that is, for a given detected ion mass, only clusters larger than a certain size can possibly contribute to the signal. This represents a significant advantage over the matrix isolation technique, where strong absorption by monomers and smaller clusters often obscures absorption peaks due to larger clusters. As an example, suppose we set the quadrupole mass filter to pass $(H_2O)_3H^+$ (m/e = 55). The smallest water cluster which could produce

this ion in the ionizer is $(H_2O)_4$, and the smallest cluster which could produce $(H_2O)_4$ by vibrational predissociation is $(H_2O)_5$. Thus, only pentamers and larger clusters can contribute to the vibrational predissociation signal measured at m/e = 55. This suggests that while we cannot hope to measure spectra of individual water clusters in this experimental arrangement, we can hope to measure trends in the cluster spectra as we adjust the cut-off of our "high-pass" filter.

Vibrational predissociation spectra were measured using four different nozzle stagnation pressures. For each stagnation pressure, the ion mass detected was chosen to be the largest mass whose signal was 10 times larger than the background after 2000 laser shots at the absorption maximum. The experimental conditions are summarized in Table 1. In all cases, the detector was positioned at a fixed angle of 4° from the molecular beam. The signal produced by the laser was recovered from the background using the counting electronics and gating scheme described previously.[25c] The laser power was measured using a power meter placed a few inches after the intersection region of the laser and molecular beams. A germanium filter masked the meter aperture and allowed reading the idler energy without attenuating the energy available for dissociating the clusters. Although both signal and idler frequencies pass through the molecular beam in this configuration, checks at the major absorption frequencies showed no dependence of the predissociation signal on the OPO signal frequency. At each frequency, the signal was accumulated for at least 2000 laser shots and normalized to the average laser power. Since a scan of 50

laser frequencies took over 4 hours, to ensure long-term stability the spectra were scanned in two directions and checked for agreement within statistical counting error. No long-term drifts in the molecular beam intensity were observed. Also, for each spectrum, the power dependence of the signal was checked at the major peaks to guarantee linearity of the predissociation yield with photon flux. The large error bars near 3550 cm^{-1} result from anomalously low idler power attributed to OH impurity in the $LiNbO_3$ crystal. For these points, the counting times were extended to ~20,000 laser shots. Finally, the power normalized signals were divided by frequency to convert from power to photon flux.

To obtain information on the dynamics of the vibrational predissociation process, angular and velocity distributions of the predissociation products were also measured at selected laser frequencies.

Results and Analysis

The water cluster vibrational predissociation spectra are shown in Fig. 3. The spectra are labelled according to the smallest polymer dissociation process capable of contributing to the detected ion mass. The difficulty in assigning a given spectrum to a unique parent species has already been mentioned. In this section, arguments will be presented which suggest that the measured spectra in Fig. 3(a)-(d) are largely due to the predissociation of the labelled species. We will also discuss the validity of equating the vibrational predissociation spectra (measured at a fixed detector angle) to the infrared absorption spectra of the hydrogen-bonded clusters. Finally, the angular and velocity distributions of the predissociation products will be used to obtain information on the dynamics of the vibrational predissociation process.

The relatively high binding energies of the water clusters compared to the photon excitation energy substantially reduces the possible vibrational predissociation channels. Using four different intermolecular potentials,[27-30] the equilibrium bond energies (D_e) relative to complete dissociation of an n-mer into n water monomers were calculated[31] and are listed in Table 2. The energetically allowed dissociation channels from the harmonic approximation zero point energy levels (D_o) for several small polymers are also listed.

There are two major energy classifications of the dissociation processes. The lowest energy channel for all polymers includes a monomer fragment and is called monomeric dissociation (MD). It is defined by the equation:

$$(H_2O)_n + h\nu \xrightarrow{MD} (H_2O)_{n-1} + H_2O \quad . \qquad (1)$$

The next energetically accessible dissociation process divides the parent cluster into two smaller clusters nearly equal in size. This channel is called complex dissociation (CD) and is defined by the equation:

$$(H_2O)_n + h\nu \xrightarrow{CD} (H_2O)_m + (H_2O)_{n-m} \quad , \; m > 1 \quad . \qquad (2)$$

The model potentials show reasonable agreement with each other for D_e values. The zero point energy corrections are substantial for each potential and vary over a much larger range. Because the model potentials were constructed without considering the D_o values, little significance will be placed on them in the current binding energy analysis. This point will be discussed in detail below.

The CD channel computed from the D_e bond energies in Table 2 is not always accessible over the frequency range probed. The simplest explanation consistent with the spectral observations discussed here and the dynamic properties presented below, would attribute all dissociations as occurring through the energetically favorable MD channel, since the time of flight and angular distributions (see below) do not change with frequency within experimental error as might be expected if a new dissociation channel became energetically accessible.

The electron impact fragmentation behavior of water clusters has not been analyzed in the literature. The exceptional stability of the H_3O^+ ion explains the dominance of the mass peaks $(H_2O)_nH^+$ in the mass spectrum. The electron bombardment ionization of the neutral $(H_2O)_n$ clusters presumably first proceeds by the ionization of a water monomer subunit. A unimolecular ion-molecule reaction follows in which the H_3O^+ ion is formed (solvated by the remaining water molecules) and an OH radical is ejected from the cluster. The dominant ionization mechanism, then, is assumed to be

$$(H_2O)_n + e^- \rightarrow (H_2O)_{n-1}\ H_2O^+ + 2e^- \rightarrow (H_2O)_{n-1}\ H^+ + OH + 2e^- \qquad (3)$$

If this simple picture were complete, each water cluster, $(H_2O)_n$, would be correlated with a single ion, $(H_2O)_{n-1}\ H^+$, in the mass spectrometer, and assignment of the vibrational predissociation spectra would be straightforward. Unfortunately, in the electron bombardment ionization process, the $(H_2O)_{n-1}\ H^+$ ion may be formed with substantial vibrational energy, such that one or more water molecules may dissociate from the cluster ion. Therefore, the mass spectrum of each water cluster, $(H_2O)_n$, also contains smaller $(H_2O)_m\ H^+$ mass peaks (where $m < n - 1$). This source of contamination makes it impossible to assign the predissociation spectra in Fig. 3 to a unique parent species by mass spectroscopy alone. The fact that this contamination can potentially be very serious is demonstrated in Figs. 3(a),(e). The two spectra shown were both measured by tuning the mass spectrometer

to H_3O^+, nominally assigned to the trimer dissociation by Eqs. (2) and (3), but using very different nozzle expansion conditions. The Fig. 3(a) spectrum was obtained with the water reservoir held at 67.5°C, giving a nozzle stagnation pressure of 209 torr (see Table 1). The H_3O^+ signal amounted to 1.2 counts/laser pulse at 3400 cm^{-1}, with 0.7 counts/pulse at $(H_2O)_2H^+$ and much less signal at any higher masses. The spectrum in Fig. 3(e) was obtained with the water reservoir held at 90°C, giving a nozzle stagnation pressure of 526 torr. Under these conditions the water beam was heavily polymerized. The H_3O^+ signal at 3400 cm^{-1} was 5.3 counts/pulse, and at least 1 count/pulse was obtained at all $(H_2O)_n H^+$ masses up to $(H_2O)_6 H^+$. While we believe that the spectrum in Fig. 3(a) is largely due to predissociation of water trimers, it is clear that the spectrum in Fig. 3(e) is heavily contaminated by fragmentation of the predissociation products of larger water clusters in the ionizer.

However, we can still set some idea of how the water cluster distribution varied with nozzle stagnation pressure by assuming that $(H_2O)_nH^+$ comes solely from $(H_2O)_{n+1}$. We list in Table 3 the pressure dependence of the ion ratios $(H_2O)_n H^+:H_3O^+$, n = 1–3. These ratios were measured by pointing the mass spectrometer directly into the water beam (after suitably reducing the first detector aperture to avoid flooding the detector). The measurements were made at low quadrupole resolution in order to minimize errors due to the mass dependent transmission of the quadrupole. In principle, the pressure dependence of the polymer species in the beam could be used to identify the signal

at a given ion mass with a particular parent beam cluster.[15] However, because of the possible complicated fragmentation of each water cluster in the ionizer, the $(H_2O)_nH^+:H_3O^+$ ratio probably does not accurately reflect the $(H_2O)_{n+1}:(H_2O)_2$ ratio in the molecular beam. Nevertheless, the ion ratios do show that the distribution becomes broader, extending to larger clusters, at higher stagnation pressures. It also appears that, for our range of experimental conditions, the cluster distribution always falls off monotonically with increasing cluster size (i.e., there are always more trimers than tetramers in the beam, more tetramers than pentamers, etc.).

To summarize the correlation of the detected ions with the predissociated parent clusters, the energetics of the vibrational predissociation of neutral clusters supports only one product channel, Eq. (1), over the complete frequency range. The ionization process is most likely dominated by Eq. (3). Therefore,

$$(H_2O)_n + h\nu \rightarrow (H_2O)_{n-1} + H_2O \qquad (4)$$

$$(H_2O)_{n-1} \xrightarrow{e^-} (H_2O)_{n-2}\, H^+ + OH + 2e^-$$

$$H_2O \xrightarrow{e^-} H_2O^+ + 2e^-$$

gives the correlation between parent clusters and the dominant observed ion masses. We emphasize again that this correlation is oversimplified, and some contamination from larger clusters is unavoidable. However, by adopting the procedure of monitoring, at each nozzle

stagnation pressure, the largest ion mass which gave a reasonable signal to noise ratio, we have tried to minimize this contamination as much as possible. In the following, we will refer to the spectra in Fig. 3(a)-(d) as the trimer, tetramer, pentamer and hexamer spectra, respectively, with the qualifications discussed above.

The spectrum of the dimer was not observed in this experimental arrangement. The monomer (H_2O^+) mass peak has a large constant background from the molecular beam[33] and a large laser correlated background from the predissociation monomer fragments of larger clusters (Eq. (4)). Under source conditions where the trimer dissociation signal at its absorption maximum was within one standard deviation of the background after 2000 shots, no signal was observed at H_2O^+ at any frequency.

At this point, we would like to ask to what extent a vibrational predissociation spectrum, measured at a fixed detector angle, may be considered equivalent to the infrared absorption spectrum of the parent cluster. As long as the mass spectrometer detects a constant fraction of the total predissociation yield over the frequency range of interest, the correspondence between the vibrational predissociation spectrum (normalized to photon flux, not power) and the absorption spectrum should be exact. To prove that the fraction of the predissociation products detected is independent of laser frequency, two conditions must be satisfied. The first condition is that the laboratory angular distribution of the products does not change in shape with a change in the exciting frequency. There are several

reasons why this condition might not be satisfied. For example, as the photon energy increases, the amount of excess energy available for fragment translational motion also increases, and the products could then be scattered into a wider laboratory angular range. However, angular scans of different masses at the major absorption peaks showed no frequency dependence within experimental error. The angular distributions will be considered in more detail later. The second condition, which is harder to verify in our present experiment, is that all predissociation events occur faster than 4 microseconds, which is the average time it takes the molecules to traverse the interaction region viewed by the detector. If the time scale extends beyond this value and is frequency dependent, some of the excited clusters will travel beyond the viewing range of the detector before dissociating and their fragments will not be counted, producing an artifically low and biased absorption signal. Lacking direct experimental determination of the predissociation lifetimes, we will assume for now that this second condition is also satisfied.

Information on the predissociation product state distributions is obtained from the laboratory angular and time-of-flight distributions of the products. An explanation of the assumptions and method used in deriving a center-of-mass product translational energy distribution from the laboratory data can be found elsewhere.[15] The experimental results, shown in Fig. 4, unequivocally show substantial internal excitation of the fragment molecules. The velocity distributions at the small angles where signal is present are not as sensitive as the

angular data in describing the energy states of the fragments. The initial, unexcited polymer beam velocity is large compared to the small center-of-mass recoil velocities of the predissociation fragments and severely convolutes any details which might be present in the laboratory time-of-flight distributions. A detectable broadening of the beam velocity distribution is observed off-axis and is easily fit with a range of center-of-mass translational energy distributions.

The angular data exhibit a steep monotonic decrease with increasing laboratory angle which can only be fit with a center-of-mass energy distribution which peaks at or near zero translational energy and rapidly decreases with increasing product translational energy. A simple analysis relating the laboratory angle, nominal beam velocity and center-of-mass velocity[15] shows that the recoil energy necessary to scatter fragments to 4° is merely tens of wavenumbers, while the particles at 10° have at most several hundred wave numbers of translational energy. The angular scans for all but the H_3O^+ peak are nearly identical. The fragmentation of the polymers under electron bombardment obscures the small differences expected, i.e., the lighter fragments should be scattered to larger angles.

Discussion

A. Spectroscopy

As a first attempt to assign the features of the water cluster spectra, normal mode calculations have been performed using water potentials which allow the intramolecular monomer bonds to distort. This was thought to be a reasonable starting point even though most potentials were tailored toward modeling the liquid phase, because the calculations by Clementi[5] show that the two body interactions dominate in the many body expansion of the liquid phase potential, and from Figure 3 it is seen experimentally that the liquid phase spectrum forms a smooth envelope for the cluster spectra. A more detailed comparison between the cluster and liquid infrared absorptions will follow below.

For each potential, the configuration of the atoms was varied using a multi-parameter minimization procedure to find locally stable polymer configurations. For the Watts potential,[27] a single minimum was found for the water trimer, a cyclic structure shown in Fig. 5b. Larger polymers had several local minima, but in each case the lowest energy configuration found was cyclic. There is no proof that these are global minima, but it is thought that any deeper minima would be within a few kcal/mole of the cyclic structures, and would differ mainly in the orientations of the hydrogen atoms protruding away from the ring structures.

At the minima, the harmonic frequencies of the normal modes were calculated using finite differences to obtain the second derivative

force constants of the potential. The six zero frequencies from the rotational and translational degrees of freedom were numerically within several tenths of a wave number of zero and the absolute accuracies of all the harmonic frequencies are well within this error limit, including the effects of finite arithmetic and slight displacements from the equilibrium position. Using the harmonic frequencies, the harmonic zero point energy (HZPE) can be obtained. The differences in energy between some of the secondary minima of the larger clusters and the cyclic equilibrium structures were within the 5-7 kcal/mole HZPE of the cyclic structures. This substantiates the expectation that the molecules would behave non-rigidly. For the Stillinger central force and polarization potentials the minimum energy configurations found by using the multiparameter minimization procedure when beginning at the cyclic structures characterizing the Watts potential were also cyclic, except for the polarization model where the sequential trimer is the most stable. Table 4 contains the normal mode frequencies for several water polymer configurations obtained using the published potential forms.

The observed absorption spectra are characterized by two features: a sharp, narrow absorption 15 cm^{-1} wide located at 3715 cm^{-1}, and a 600 cm^{-1} broad absorption extending from 3000-3600 cm^{-1} with an approximate 150 cm^{-1} superimposed fine structure. The sharp peak is midway between the gas phase monomer symmetric (3657 cm^{-1}) and antisymmetric (3756 cm^{-1}) stretching vibrations and is representative

of an uncoupled, non-hydrogen bonded intramolecular O-H stretch. For comparison, the OH stretch in HOD occurs at 3705 cm^{-1}. This narrow band is also what would be expected for the free hydrogens of the equilibrium ring structures determined in the energy minimization calculations. If neither hydrogen atom of a particular water molecule is involved in hydrogen bonding, there should appear two absorption peaks correlating to perturbed symmetric and antisymmetric stretching frequencies for this "hydrogen accepting" monomer. The single sharp peak is taken as evidence that the isolated polymers containing three or more molecules are cyclic with at least one hydrogen atom of each water molecule hydrogen bonded.

Additional experimental evidence for the cyclic structures is given by the small to undetectable dipole moments of water polymers in a molecular beam polarity study.[34] For the polarization model of Stillinger the dipole moments are computed, and Table 5 contains the values for the minima displayed in Fig. 5. The small dipole moment experimentally observed for the trimer can be rationalized from the calculations to originate in the staggered out-of-plane configuration of the free hydrogens. If this trend persists, one would predict that the odd polymers would show a small dipole moment, while even polymers, with approximate S_n symmetry would have a vanishingly small one. The dipole moments from the other potentials depend only on the fixed charges and final geometry. They are included in Table 5 for completeness.

The calculated harmonic normal mode frequencies of the Watts potential show the tight frequency grouping of the free hydrogens, midway between the calculated monomer normal mode frequencies obtained with the same potential model. The Stillinger potentials show a blue shift relative to the Stillinger monomer frequencies with little grouping. This is presumably a result of the compromise the Stillinger model was forced to make when attempting to fit with the same form of the O-H interaction potential both the infrared absorption frequencies and electrostatic properties of the monomer. The potential was not sufficiently flexible to enable an exact fit to all of these observables.

The second major feature of the spectra--the broad, hydrogen bonded absorption--is not as easily understood. The broadness of the hydrogen bonded infrared spectra has been experimentally well documented.[35] The theoretical models which have explained the extensive absorption in other systems (such as carboxylic acid dimers[36]) conclude that a strong coupling picture involving at least the hydrogen bond and intramolecular stretching coordinates common to the hydrogen bonded hydrogen atom is necessary. Additional complications may arise from the resonant first overtone of the intramolecular bending frequency near 3200 cm^{-1}. The breadth of other hydrogen bonded systems besides water have been explained without resorting to a Fermi resonance picture, so the fundamental coupling mechanism producing the broad absorption is taken to involve the O . . . H-O group, with Fermi

resonance (involving $2\nu_2$) possibly accounting for a portion of the intensity pattern near 3200 cm^{-1}.

Sceats[37] has calculated the effect of the bending overtone interaction on the fundamental infrared stretching region in liquid water. The dynamical perturbation caused by the intermolecular $O_i \ldots O_j$ motions distribute the Fermi resonance over a broader frequency range. What would have appeared as a narrow dip in the absorption spectra at the overtone frequency is instead broad and diffuse. The observed dip at 3250 cm^{-1} in the cluster spectra may be such a resonance.

Even without an exact quantum number assignment of the vibrational bands, the similarity of the frequencies and number of bands for the series of polymers measured means that the basic near neighbor interactions dominate, once the cyclic structures are formed. The trimer differs from the larger cyclic structures in the calculations principally from its more strained configuration, reflected in more non-linear hydrogen bonds and a higher zero point energy.

The calculations presented here are too simplistic to decide if this is the only plausible explanation for the cluster spectra. In the Marechal-Witkoski[36b] or Robertson/Coulson[18] strong coupling models, if there should be a change in the average intermolecular cluster geometry when the intramolecular stretching motion is excited, the intensity pattern of the combination series involving the hydrogen bond stretching motions may not peak at the fundamental $0 \rightarrow 1$ intramolecular transition. This effect has been most clearly observed

in the $HCl\text{-}O(CH_3)_2$ complex.[38] If this geometric distortion is responsible for the observed band series of the water clusters, the 3200 cm^{-1} band could be assigned to the fundamental intramolecular stretching transition, with the bands at 3350 and 3550 cm^{-1} a combination series involving a 150-200 cm^{-1} hydrogen bond motion. The 150-200 cm^{-1} band splitting is the correct magnitude for the hydrogen bond stretching frequency. Whether a single hydrogen bond frequency is responsible for both bands is not clear. The above assignment for the fundamental frequency has the appealing feature that the 3200 cm^{-1} transition coincides with the peak infrared absorption of ice Ih.

A proper treatment of the large amplitude intermolecular motion is necessary before the strong coupling picture can be adequately tested. If more than one local minimum structure is accessible to the ground state wave function, it is not known how the infrared spectra would be affected. For example, the variation of zero point energy may be sufficient to allow sampling a linear configuration by breaking the hydrogen bond forming the ring structure, or there might be a concerted process involving the interchange between free and bound hydrogens without passing through the linear configuration. Whether such loose complexes can be modeled as the sum of spectra of each configuration, weighted by the probability of that configuration in the zero point wave function, is not known.

Liquid water spectra have been quantitativly analyzed by assuming the Badger-Bauer relation between frequency and bond length to be operative.[39] Using an empirical curve of frequencies and bond

lengths, the distribution of oxygen-oxygen distances in the liquid has been calculated from the infrared spectra. The near Gaussian shape of the liquid infrared spectra does not show any of the fine structure seen in the polymer spectrum, although the existence of four components comprising the broad infrared absorption can be inferred from curve decomposition. These four bands were then suggested to be characteristic of water molecules bound to different numbers of or in different ways to neighboring water molecules.

Additional evidence for distinct water bonding types in the liquid have been derived from the temperature dependence of the first stretching overtones. Using the overtone region to separate the congested fundamental infrared bands, Luck[40] and others[41] have performed many experiments which show clear isosbestic behavior in this region, suggesting an equilibrium between at least two species of water molecules. Recently Sceats[42] has reinterpreted the overtone region using a quantum mechanical picture, showing that reasonable values for the electrical and mechanical anharmonicities in the liquid phase can explain the observed isosbestic behavior. Consequently, the apparent isosbestic behavior is not a sufficient condition for the mixture model of water.

More recently, Byer et al.[43] have measured the depolarization CARS spectra of liquid H_2O and have observed spectral structure in the regions of the bands observed here, excepting the free O-H stretch. Their experiment conclusively shows that the broad liquid absorption is composed of several overlapping vibrational bands. Despite the

fact that the room temperature infrared bands are so overlapped to give the appearance of a single broad band, the depolarization CARS experiment can resolve these features using the different depolarization ratios of the vibrational transitions. The cooling of the water clusters in the molecular beam expansion and mass selective detection enables the features to be resolved in the work reported here. With this clear evidence for substructure in the liquid phase spectrum, a confident analogy can be drawn between the interactions present in the gas phase clusters and the liquid.

Matrix isolation results beginning with the pioneering work of Pimentel have used the concentration dependence of spectral features to assign bands to particular water polymers. Host materials have included Ar, N_2, and D_2.[44] The dimer has attracted the most attention because the original N_2 matrix work suggested a cyclic structure for the dimer, contrary to later theoretical calculations. Subsequent higher resolution matrix studies have identified the expected number of intramolecular vibrations for a trans-linear structure, the same given by the most extensive quantum mechanical calculations, although the D_2 matrix appears exceptional, supporting only a cyclic structure.

Molecular beam electric resonance spectroscopy[34] has definitely established that the gas phase dimer is stable in the trans-linear form. Whether the cyclic structure is stabilized with respect to conversion to the trans-linear form is not known from these beam experiments, since the cyclic structure would be non-polar and not

observed in the usual experimental arrangement. The change in the zero point energy from theoretical models would appear sufficient to interconvert the two forms even though there might exist a mechanical barrier. The conclusion seems to be that the difference in energy of different water dimer geometries is insufficient to result in one matrix dimer independent of the host material.

A second problem with neglecting host-guest interactions in the matrix work has been observed in HCl isolated in Ar matrices. Here the rare gas-HCl interactions have been extensively modeled. In these studies[45] it was concluded that HCl monomers located in near neighbor vacancies could perturb each other's vibrational frequencies. Such "pseudo-dimers" appear before the onset of higher polymerization. In the matrix studies of water dimer and higher polymers, no corresponding treatment for the matrix perturbations has been given. The stretching features observed near the H_2O monomer bands might originate from "pseudo-dimers." The demonstrated variation of water dimer geometries in various host materials and the possibility of "pseudo-dimers" places some doubt on the certainty of the current matrix assignments with regard to determining the gas phase structure until a quantitative treatment of the water-matrix interaction is available.

The vibrational predissociation spectra obtained in this study disagree with some of the matrix assignments for trimer and multimer spectra. Primarily, the gas phase clusters are all seen to absorb over the same frequency range, principally distinguished by variations in

intensity, not frequency. It is difficult for the matrix technique to distinguish between different species absorbing at the same frequency. The molecular beam method with mass selectivity can limit the size of the parent polymers which are measured, and to some degree circumvents this problem.

For the assignments of the matrix trimer spectra to be correct, the matrix trimer would either have to be trapped in a different intermolecular geometry than exists in the gas phase (such as a linear arrangement), or the contributions from higher polymers in the present molecular beam experiments dominate the signal assigned to the trimer. However, the trend with decreasing beam polymerization (lower nozzle stagnation pressures) in the series of spectra reported here indicates a decrease in intensity of the 3550 cm^{-1} band relative to the 3200 and 3350 cm^{-1} bands. The 3550-3700 cm^{-1} frequency range in the matrix work is the region of the assigned trimer bands with the 3300 cm^{-1} range assigned to tetramer and higher clusters. Thus, the pressure dependence of the H_3O^+ spectrum in the molecular beam work is in the opposite direction to be consistent with the assignments obtained in the matrix work.

The infrared spectrum of ice has been used as evidence against the theories supporting the intrinsic breadth of hydrogen bond absorptions. Using a dilute isotopic sample of HDO in D_2O or H_2O crystals, narrow, 50 cm^{-1} wide absorptions are seen in the OH and OD regions respectively.[46] If this width is the basic band profile, then the dynamic coupling in the solid must be quite different than in the liquid or

gas phase polymers or the disruption of symmetry by isotopic substitution has a large effect. The different phases of ice[47] show noticeable variation in the infrared spectra, and the special near translational symmetries of the solid, absent in the liquid and clusters, point to a delicate balance of short- and long- range forces. As noted above, the 3200 cm^{-1} cluster band is coincident with the peak absorption in the Ih phase of ice. If the two bands represent the same approximate normal coordinates, one can conclude that the tetrahedral intermolecular arrangement in the solid, and the cyclic gas phase polymers have similar hydrogen bonded intramolecular stretching potentials. In other words, the hybridization of the oxygen atoms in water molecules acting both as a hydrogen bond donor and acceptor is similar whether one or both pairs of hydrogen atoms and lone pairs are bonded, so that the bonds are decoupled.

From the similarity of the liquid water and cluster spectra, we conclude that small, cyclic polymers form an excellent zeroth order model for explaining the infrared absorptions of liquid water. To date, the search for simple functional potential forms to model liquid/solid behavior has concentrated on comparing the results of molecular dynamics simulations to properties such as radial distribution functions, crystal structure, sublimation energy, etc.[5a-c,48a,b,2,49-59] McDonald and Klein[48a] used the Watts central force model based on fitting known monomer/dimer properties and found a disappointingly poor fit to liquid properties. Similarly, those potentials based on bulk

phase properties, most notably the Stillinger-Rahman central force potential, give poor agreement with gas phase properties such as second virial coefficients and dimer geometries.[49] It has been suggested,[2] therefore, that large, non-additive, many body effects in water may preclude the existence of a simple central force model which explains gas phase and cluster properties as well as liquid/solid behavior.

Perhaps the key to this problem is contained in the cluster spectra shown here. If one takes the known results for the infrared spectra of water dimers from matrix isolation work[44] or molecular beam experiments,[58] there is observed to be a dramatic spectral change between the dimer and trimer species. The dimer spectra are not as intense as the trimer spectra, are confined to a narrower frequency range (3530-3715 cm^{-1}), and bear little similarity with liquid water. In contrast, the trimer and higher clusters absorb over the complete range that liquid water does. To concentrate on dimer properties may then be misleading if one wishes to predict liquid properties. Potentials based on the infrared spectra of trimers and higher clusters measured in this work should have better success in describing liquid behavior while retaining contact with experimental results which are simpler to calculate and ascribe to specific potential surface features. The previous lack of agreement between potentials[2] based on gas or bulk phase properties indicates that the spectral information presented here is complimentary to known results and the range of potentials which describe both satisfactorily ought to be limited.

Quantum mechanical calculations can aid in distinguishing the various band assignment possibilities. From the sophisticated SCF calculations by Clementi[5] using large basis sets, it was concluded that within the frozen monomer approximation, the non-additive three body interaction is only 10 percent of the pair interaction energy and shows no pronounced directional character. This would imply that the Watts potential should show excellent agreement with experiment, predicting the pair interaction properties quite well. Correcting the calculated dimer "intramolecular" frequencies from the Watts model by the previous procedure of insuring that the calculated and observed monomer transitions agree, Table 6 shows the rather remarkable agreement between the Watts model normal mode frequencies and the assigned matrix transitions. Agreement is all the more interesting because Watts did not report deliberately fitting his model to these frequency data. The scaling procedure is expected to be valid since the intramolecular potential is the same as for the gas phase monomer, except that in the dimer, the atoms are vibrating about a displaced equilibrium position. The anharmonicity of the intramolecular stretches for the polymers is then equal to that of the monomer to first approximation. Least square fits are also shown to indicate "best fits" and give some additional indication of the anharmonicity contribution resulting from intermolecular bonding.

The cyclic polymers of the Watts model, however, are seen to have normal modes in the same range as the dimer. Therefore, the empirical pair potential does not predict a lowering of the hydrogen bonded

intramolecular harmonic frequency upon forming a cyclic structure. The calculations show, therefore, that changes in the reduced mass cannot account for the experimentally observed red shifts. Non-additive effects must be quite important for the intramolecular properties, so far unexplored in theoretical calculations within the frozen monomer approximation.

The frozen monomer geometry approximation also overlooks the effect upon the energetics of the intramolecular zero point motion. As shown in Tables 2 and 4, the total harmonic zero point energy (HZPE) accounts in all cases for at least 25 percent of the binding energy. If the assignment of the 3200 cm^{-1} feature to a fundamental vibration is correct, then for a cyclic n-mer, this contributes n*(3715-3200)/2 cm^{-1} or n*.7 kcal/mole of stabilization energy relative to the HZPE of the separated water monomers. Besides reducing the amount of inter-molecular bonding needed to produce the same total zero point binding energy, D_o, configurations of the polymer which have less red shifted frequencies will be relatively higher in energy. A quantitative quantum mechanical treatment of the intermolecular potential at the 10 percent level of error must include an estimation of the HZPE, both for the inter- and intra-molecular motions.

An important theoretical calculation to elucidate the above transition from dimer to trimer behavior is an estimation of the effect of configuration interaction upon the intramolecular frequencies. The possible ionic-covalent resonant structures especially deserve treatment. The $D'A_1$, and $C'B_1$, states of H_2O have vibrational frequencies

at 3268, 3335 cm^{-1} and 3170, 3224 cm^{-1} respectively for the ν_1 and ν_3 vibrations.[61] The bond length for the $C'B_1$, state is 1.01 Å with a bond angle of 106^{o}.[61] Both states are of C_{2v} symmetry. The similarity in structure between the H_2O monomer in the ground and these excited electronic states which involve an excitation of the "lone pair" electrons would indicate a favorable geometric orientation in the clusters for mixing these states. The vibrational frequencies are remarkably near the 3200 cm^{-1} band assigned here to a fundamental cluster vibration.

The difference in intramolecular frequencies in the dimer and the cyclic polymers can occur from two effects. First, the dimer in the trans-linear configuration has two distinguishable water monomers--one donating, one accepting a hydrogen atom. In the cyclic polymers, the water molecules are nearly identical, each monomer acting both as a donor and acceptor. The resonance stabilization resulting from the indistinguishability of the water monomers might substantially lower the energy. Secondly, for the "charge transfer" cluster configurations, the cyclic structures gain additional stabilization from the solvation energy of the H_3O^+ and OH^- ions by the remaining water molecules as shown in Figure 6. From the $(H_2O)_n \cdot H_3O^+$ and $(H_2O)_n \cdot OH^-$ energetics, it is seen that the biggest jump occurs for $n = 1$, after which the additional stabilization energy from successive water molecules is additive. This is expected to give the "ionic" forms of the cyclic trimer approximately 1.5 eV more stabilization over the

equivalent dimer form, without including the effect of the resonant ionic structures available to the trimer and not the dimer as a result of the equivalence of the water molecules in the cyclic structures. If this conjecture on the importance of C.I. in understanding the intramolecular vibrations is true, that would also imply that the point charges placed on the oxygen and hydrogen atoms of current analytical models must be made parametrically dependent on the intermolecular orientations and distances.

Until this point, the comparison of the data has concentrated on comparison with simple analytic forms which were not designed to predict the fundamental vibrational spectra of gas phase clusters. Sceats and Rice[59] have considered a wide range of water properties and proposed that to understand the infrared fundamental and overtone absorption spectra of ice, only a single parameter, η, which modifies the two quadratic stretching constants, K_{rr} and $K_{rr'}$, can explain the observed shifts. In their analysis of solid state data, they could assume that each water molecule and each O-H bond were approximately equivalent. In the polymer spectra, this is known not to be true. Therefore, to use their results as a first refinement, a geometric relation between the value of η for each O-H bond in the cluster environment must be defined. The goal is to introduce an additional term into the total potential which depends explicitly on both the intramolecular and intermolecular coordinates in such a way as not to spoil the basic agreement found for the dimer using the Watts potential. This means that the new interaction term must be

essentially a three body term which affects only those hydrogen motions involved in hydrogen bonding. The work of Sceats and Rice offers no suggestion as to the physical origin of the changes which result in the force constants of ice having the particular η dependence. The parameter merely serves to reproduce, with least modification of the water molecule force field, the observed features. Consequently, we shall adopt a similar phenomenological approach and first demonstrate that a reasonable value of their parameter, introduced appropriately, can shift the hydrogen bonded O-H stretches into agreement with experiment. This is simply accomplished by defining the η parameter for the ith hydrogen atom as

$$\eta_i = C \sum_{j \neq i} \cos^2(\theta_{ij}/2)/r^6_{H_iO_j} \qquad (5)$$

where θ_{ij} is the angle between the $H_i - O_i$ intramolecular axis and the $O_i \ldots O_j$ intermolecular axis, $r_{H_iO_j}$ is the distance from the ith hydrogen atom to the jth oxygen atom, and C is a constant. At the Watts trimer potential minimum, it was found that if C 50, the hydrogen bonded stretching frequencies agree well with the harmonic values given by Sceats and Rice for ice I (3550 cm^{-1}). The free hydrogen fundamental frequencies decrease by only a few wavenumbers when the η dependence is included. This demonstrates that a simple functional form can be found for η which preserves the separation of the cluster proton types, and will also correlate to the value for ice I. As given, the shift will occur for the dimer as well, unless this

term is included in only clusters containing three or more molecules. The problem is once again that the physical reason behind why the cyclic polymers are shifted, whereas the dimer is not, is unknown. There is no way of knowing then how to incorporate the η parameter in a reasonable way (for example, if η depends on charge transfer or polarization effects) and how these affect the force constants.

The intramolecular properties measured here are indirectly related to the intermolecular interactions. Since the fundamental monomer vibrations are, in principle, understood quite well, the differences between the hydrogen bonded intramoleculer vibrations and the free monomer vibrations will provide information on the charge separation within each water moleculer. This will, in turn, constrain the form of the pair interactions between water molecules. Agreement with the high frequency infrared properties does not imply that a particular potential's intermolecular properties will be correctly predicted. A large number of diverse properties must be considered before deciding if a potential is superior to another.

An additional characteristic feature of hydrogen bonding is a large increase in the absorption intensity in the O-H stretching region. The predissociation spectra reflect this by comparing the ratios of the integrated free and hydrogen bonded absorption bands. The oscillator strength of the free O-H bands is expected to be approximately proportional to the cluster size. The progressively smaller free O-H peak in the series of normalized spectra indicates a substantial increase in the absorption strength of the hydrogen bonded

O-H groups. The quantities $|d\mu/dQ|^2$ were calculated (where Q is a normal coordinate) for the various potential models to compare with the measured integrated band intensities and are included in Table 4. The first order expansion of the dipole moment function is meant to serve as an order of magnitude predictor of the vibrational band intensities.

B. Dynamics

The experimental results show that predissociation is occurring on the microsecond time scale, with a negligible amount of energy appearing in fragment translational motion. From energy balance, this implies that the predissociation products are vibrationally and/or rotationally excited. With this qualitative information on the dynamics, what can be learned about the predissociation mechanism?

The two current theories of vibrational predissociation by Ewing and Beswick/Jortner have only addressed the case of binary complexes. In Ewing's model, the dissociation is reduced to a simple one dimensional treatment. The remaining internal coordinates are considered only as a "heat bath" which reduce the amount of energy which can appear in the translational coordinate for the given product quantum states. The lifetimes are shown to have an exponential dependence on the translational energy and for the hydrogen bonded dimers modeled, lifetimes in the microsecond range occur only if the rotational excitation is substantial. No explicit account of angular momentum conservation is included, except in determining correlations of product

rotational states with initial cluster states. Interaction between the overall complex rotation with the internal motions correlating to the free monomer rotations is neglected.

The Beswick/Jortner model introduces the coupling between the intramolecular and intermolecular motions in a more consistent manner. The decay rate of an initial vibrational state is the product of an intermolecular and intramolecular term. The intermolecular term contains the exponential dependence on the translational energy as in the Ewing model, while the intramolecular term expresses the coupling between the initial and final monomer vibrational states. The intramolecular factor is expected to decrease rapidly with the number of quantum changes between initial and final states. For example, in $(N_2O)_2$, the competition between these two factors predicts a different product state distribution than Ewing's model based on a linear coupling term of the intramolecular coordinates. This occurs because a higher order intramolecular coupling term results in a final state whose translational energy gap is smaller than the final states accessible through lower order intramolecular processes. The Beswick/Jortner model has not been applied to hydrogen bonded binary complexes, but it is reasonable to assume that the observed lifetimes and energy distributions could be accounted for by their model.

A third possibility is that the coupling is sufficiently strong in the water clusters that a statistical product energy distribution is more appropriate. These models (RRKM or RRK), for systems with many vibrational degrees of freedom and without exit barriers, are known to

have translational energy distributions which peak at zero and drop rapidly with increasing energy.

To decide which of these models is suitable, three calculations have been performed using the Watts potential to investigate the predissociation mechanism. The first consists in determining a local, minimum energy dissociation coordinate (LDC). The minimization computer program was modified to allow the distance between two of the oxygen atoms to be fixed at one value while varying the remaining atomic positions to minimize the total energy. Starting at the minimum energy configurations for the dimer, trimer and tetramer, the LDC's are shown in Fig. 7.

The dimer dissociation is straightforward, resembling a simple diatomic molecule. The trimer, however, shows a two step process to dissociation. First, the ring structure is broken (R = 2.75Å to 5.50Å) then a monomer dissociates from the cluster in a similar manner as in the dimer. The tetramer indicates more exotic behavior which also should be characteristic of larger clusters. Curve C in Fig. 7 shows the dissociation when two adjacent water molecules of the tetramer are pulled apart. The plateau is again characteristic of the opening of the cyclic equilibrium structure. However, the dissociation of the linear tetramer does not proceed concertedly with the reforming of the cyclic trimer. The configuration of the trimer sub-unit near dissociation is extended and far removed from its equilibrium geometry. It is expected, therefore, to contain substantial internal energy.

Repeating the calculation in the reverse direction (adding a monomer to a cyclic trimer) results in curve D of Fig. 7. The reverse path has a relative minimum with the approaching water monomer bonded to one of the free OH groups of the cyclic trimer. The energy barrier to adding this water to form a cyclic tetramer from this relative minimum is ~0.5 kcal. The "hysteresis" of the two paths is a result of the numerous local minima on the potential surface. Since the LDC is generated by small sequential displacements (~0.2Å) of the oxygen-oxygen distance, these curves are not global minima.

The LDC's suggest that there are two timescales analogous to the liquid phase relaxation measurements, the hydrogen bond breaking rate and the cluster dissociation rate. The hydrogen bond breaking rate will be normally that of the transfer rate of the photon energy from the high frequency "intramolecular" optically excited vibrations into the intermolecular motions. This process should be describable by the vibrational predissociation theories of Ewing or Beswick/Jortner. The second time scale, that for dissociation of the clusters once the energy has been coupled into the intermolecular motions, is not expected to be negligible. The LDC's indicate that the cyclic polymers must undergo substantial configurational changes before dissociation. This is expected to strongly couple all of the allowed exit channels satisfying energy and angular momentum conservation.

To explore this strong coupling in the exit channels, several molecular dynamics calculations have been performed. The first model for the dissociation began with the tetramer. The initial positions

were chosen to correspond to the minimum energy cyclic configuration. When the energy was set equal to the HZPE, and the trajectories observed for what bonding configurations were included in the zero point motion, it was found that the ring structure was preserved with no interchange of the hydrogen bonded and free OH groups. Therefore, the initial configuration of the polymers could be fixed at the cyclic minimum without substantial error, since the gross bonding topology was satisfied. The velocities were chosen randomly according to a Boltzmann distribution with a temperature of 100°K. The residual velocity components in the zero angular momentum frame were scaled so that this "internal" kinetic energy equaled the sum of the HZPE and photon energy. The original rotational motion was then added back on, thus allowing the internal vibrational energy to be constant, and independent of the rotational temperature. This accounts for the presumed disequilibrium between the vibrational and rotational degrees of freedom of the polymers produced in the adiabatic beam expansion. The trajectories were integrated using the CLAMPS[62] simulation package and displayed on the NRCC interactive graphics system.[63]

Twenty trajectories were followed for 30 picoseconds with no dissociation. Even though the bonding topology changed every few picoseconds between cyclic, linear, tetrahedral, and similar configurations, and the effective temperature of the cluster was 2200°K, the heat capacity was still sufficiently large to insure that 1500 psecs. Subsequently, three sets of 50, 20 picosecond trajectories were followed for the water dimer. The rotational

temperatures for these runs were 10°K, 100°K, and 200°K, the total internal energy fixed at 3000°K (which is the sum of the photon energy and HZPE), and the minimum potential energy configuration chosen as the starting configuration. The decay curves are shown in Fig. 8. Additionally, 50 trajectories were run in which the hydrogen bonded proton was extended along its O-H intramolecular bond axis so that it had 10 kcal/mole of potential energy. This was meant to simulate the time it takes for the high frequency vibrational energy to couple into the low frequency motions. None of the trajectories for this last set dissociated even though for several of the trajectories, the energy was seen to be transferred into intermolecular motions. The conclusion from these computer studies is that the lifetime of the clusters is composed of two contributions: the relatively slow energy transfer time from the high frequency modes into the intermolecular cluster modes, and the decay time of the excited cluster (in which the energy is distributed progressively throughout the cluster) into products. The primary energy transfer time is expected to decrease with increasing cluster size since the number of internal energy states resonant with the optically excited state will increase (the energy gaps approach zero), while the decay time to products after the energy transfers from the optically excited state will increase with cluster size as the effective heat capacity increases.

Finally, RRKM calculations were attempted for a series of points along the LDC, but the results indicated much too short lifetimes compared to classical trajectory calculations. For these small systems in which rotational motions are nearly unhindered in the critical

configuration, it is difficult to obtain reasonable values for the vibrational frequencies from simple "normal mode" type analyses. On the other hand, with the level of excitation being not much higher than fundamental intramolecular vibrational energies and the hydrogen bond dissociation energy, one would expect dynamic factors to be more important than statistical ones.

Summary

Measurements on the vibrational predissociation of water clusters have shown that the process is occurring on the microsecond timescale or faster. The measured angular and velocity distributions of the fragments indicate no detectable variation with excitation frequency between 3200 and 3700 cm^{-1}, partially a consequence of the small amount of excess energy released into translation. This is in agreement with the qualitative predictions of the Ewing and Beswick/Jortner models for vibrational predissociation which favor internal excitation of the fragments for predissociations on this time scale, although these models have only been directly applied to binary clusters.

The infrared spectra obtained show a pronounced similarity with the liquid for clusters containing three or more water molecules. Presumably, this is a result of the cyclic structures of these polymers, where each water molecule is acting both as a hydrogen bond donor and acceptor. This last conclusion has been important in explaining the poor agreement between the potential models based on dimer properties and those based on liquid or solid properties. The modifications to the intramolecular potential based on the work by Sceats shows that physically reasonable models can reproduce the gross red shifts without modifying the intermolecular force fields. This decoupling of the intramolecular and intermolecular forces to first order should enable most properties to be fit in a systematic way.

The analysis presented here for H_2O should also explain the observed features of HF clusters,[64] which show the same dramatic

change between the dimer and trimer and provide additional evidence for the favored cyclic equilibrium structures of hydrogen bonded clusters containing three or more molecules.

Several issues still remain unsolved. First of all, the reasons for the breadth of the hydrogen bond absorption is unexplained, as well as the exact assignments of the bands observed. The rotation-vibration coupling of the hydrogen bonded bands[38] can be used to derive approximate band contours. The recent classical linear response theory methods of Behrens and Wilson,[60] if extended to handle combination and overtone bands, will enable the larger cluster spectra to be calculated. Although there are uncertainties in the dipole moment and potential functions, the special trends with cluster size outlined in these experiments might be properly accounted for, considering the large amplitude motion of these clusters, by the classically based spectral response theory.

Experimentally, measurements are in progress with the greater sensitivity of the coaxial beam geometry[15] to study the (D_2O, HDO, H_2O) mixed clusters. The changes in frequencies should indicate the role of Fermi resonance in some of the bands. Also, if the extensive energy sharing among the low frequency intermolecular motions and the intramolecular vibrational degrees of freedom before dissociation, as indicated in the classical trajectory calculations, reflects the true cluster dynamics, a study of very large clusters may reveal a substantial increase in the dissociation lifetime.

Acknowledgments

Professor Bob Byer and his research group have provided immeasurable help in the design and operation of our OPO.

The normal mode calculations were modeled on the procedure described by Jack Owiciki. His comments enabled us to quickly implement our own program.

David Ceperley and the NRCC coupling staff are thanked for supplying computer time and software for the molecular dynamics calculations.

This work was supported by the Director, Office of Energy Research, Office of Basic Energy Sciences, Chemical Sciences Division of the U.S. Department of Energy under contract No. W-7405-Eng-48 and the Assistant Secretary for Nuclear Energy, Office of Advanced Systems and Nuclear Projects, Advanced Isotope Separation Division, U.S. Department of Energy under contract No. W-7405-Eng-48.

References

1. J. A. Barker, R. A. Fisher and R. O. Watts, Mol. Phys. 21, 657 (1970).
2. I. R. McDonald, M. Klein, Dis. Fara. Soc. 66, 48 (1978).
3. J. R. Rowlinson, Trans. Fara. Soc. 47, 120 (1951).
4. (a) F. H. Stillinger, J. Chem. Phys. 57, 1780 (1972), (b) F. H. Stillinger, J. Phys. Chem. 74, 3677 (1970).
5. (a) G. Lie, E. Clementi, M. Yoshimine, J. Chem. Phys. 64, 2314 (1976).
   (b) G. Lie, E. Clementi, ibid, 62, 2195 (1975).
   (c) H. Kistenmacher, H. Popkie, E. Clementi, R. O. Watts, ibid, 60, 4455 (1974).
   (d) H. Popkie, H. Kistenmacher, E. Clementi, ibid, 59, 1325 (1973).
   (e) O. Matsuoka, E. Clementi, M. Yoshimine, ibid, 64, 1351 (1976).
   (f) H. Kistenmacher, G. Lie, H. Popkie, E. Clementi, ibid, 61, 546 (1974).
   (g) E. Clementi, W. Kolos, G. Lie, G. Ranghino, Int. J. Quant. Chem. 17, 377 (1980).
6. J. A. McCammon and M. Karplus, Ann. Rev. Phys. Chem. 31, 29 (1980).
7. A. Herrmann, E. Schumacher, L. Wöste, J. Chem. Phys. 68, 2327 (1978).
8. D. Levy, Adv. Chem. Phys. XLVII, 323-362 (1981), Wiley and Sons.
9. M. Van Thiel, E. Becker, and G. Pimentel, J. Chem. Phys. 27, 486 (1957).
10. V. B. Mann, T. Neikes, E. Schmidt, W. Luck, Berichte der Bunsen-Gesellschaft 78, 1236 (1974).

11. See Chapter 29, "The Hydrogen Bond in Ice," E. Whalley in The Hydrogen Bond, eds., P. Schuster, G. Zundel, and C. Sandorfy (North-Holland, Amsterdam, 1976).

12. (a) S. Rice, C. G. Veakatesh, J. B. Bates, J. Chem. Phys. 63, 1065 (1975).

(b) N. Bergren, D. Schuh, M. Sceats, S. Rice, ibid, 69, 3477 (1978).

(c) T. Siuakumar, S. Rice, M. Sceats, ibid, 69, 3468 (1978).

(d) T. C. Siuakumar, S. Rice, M. Sceats, D. Schuh, Chem. Phys. Lett. 48, 212 (1977).

(e) J. Wenzel, C. U. Linderstrom-Lang, S. Rice, Science 187, 428 (1975).

(f) R. McGraw, W. Madden, S. Rice, M. Sceats, Chem. Phys. Lett. 48, 219 (1977).

(g) R. McGraw, W. Madden, S. Rice, M. Sceats, J. Chem. Phys. 64, 3483 (1978).

13. (a) R. McGraw, W. Madden, S. Rice, M. Sceats, J. Chem. Phys. 69, 3483 (1978).

(b) R. McGraw, W. Madden, S. Rice, M. Sceats, ibid, 69, 3497 (1978).

14. M. Morse, S. Rice, J. Chem. Phys. 74, 6514 (1981).

15. M. F. Vernon, J. M. Lisy, H. S. Kwok, D. J. Krajnovich, A. Tramer, Y. R. Shen, and Y. T. Lee, "Vibrational predissociation of benzene dimers and trimers by the crossed laser-molecular beam technique," J. Phys. Chem., in press and references therein.

16. B. I. Stepanov, Nature 157, 808 (1946).

17. D. Hagen, J. L. Kassner, J. Chem. Phys. 61, 4285 (1974).

18. (a) C. A. Coulson, G. N. Robertson, Proc. Roy. Soc. London A 337, 167 (1974).

(b) C. A. Coulson, G. N. Robertson, ibid, A342, 289 (1975).

(c) G. N. Robertson, ibid, A286, 25 (1977).

19. G. Ewing, J. Chem. Phys. 72, 2096 (1980).

20. J. A. Beswick and J. Jortner, Adv. Chem. Phys., vol. XLVII, 363 (1981).

21. B. B. Owen, Robert C. Miller, Clifford E. Milner, Harold L. Logan, J. Phys. Chem. 65, 2065 (1961).

22. J. C. Hindman, A. J. Zielen, A. Svirmickas, M. Wood, J. Chem. Phys. 54, 621 (1971).

23. K. E. Larsson, V. Dahlborg, Physica 30, 1561 (1964).

24. C. J. Montrose, J. A. Bucaro, J. Marshall-Coakley, T. A. Litovitz, J. Chem. Phys. 60, 5025 (1974).

25. (a) M. J. Coggiola,, P. A. Schulz, Y. T. Lee, Y. R. Shen, Phys. Rev. Lett. 38, 17 (1972).

(b) E. R. Grant, M. J. Coggiola, Y. T. Lee, P. A. Schulz, Aa. S. Sudbo, Y. R. Shen, Chem. Phys. Lett. 52, 595 (1977).

(c) Aa. S. Sudbo, P. A. Schultz, Y. R. Shen, Y. T. Lee, J. Chem. Phys. 69, 2312 (1978).

26. S. Brosnan, R. Byer, IEEE J. Quantum Elec. QE-15, 415 (1979).

27. R. O. Watts, Chem. Phys. 26, 367 (1977).

28. (a) H. Lemberg. F. Stillinger, J. Chem. Phys. 62, 1677 (1975).

(b) F. Stillinger, A. Rahman, ibid, 68, 666 (1978).

29. (a) F. Stillinger, C. David, J. Chem. Phys. 69, 1473 (1978).
(b) F. Stillinger, C. David, ibid, 73, 3384 (1980).

30. J. Owicki, L. Shipman, H. Scheraga, J. Phys. Chem. 79, 1794 (1975).

31. NPL Subroutine BCNDQ1-Quasi Newton algorithm to find the minimum of a function of N simply bounded variables using function values only.

32. C. Y. Ng, D. J. Trevor, P. W. Tiedemann, S. T. Ceyer, P. L. Kronebusch, B. H. Mahan and Y. T. Lee, J. Chem. Phys. 67, 4235 (1977).

33. The low pressure expansion conditions result in poor speed ratios for the molecular beam. This velocity spread results in collisions between beam molecules with small angles of deflection. When these collisions occur in the intersection region viewed by the detector, they contribute the largest component to the mass spectrometer background at small detector angles.

34. (a) T. Dyke, K. Mack, J. S. Muenter, J. Chem. Phys. 66, 498 (1977).
(b) T. Dyke, J. S. Muenter, ibid, 60, 2929 (1974).
(c) T. Dyke, J. S. Muenter, ibid, 57, 5011 (1972).
(d) J. A. Odutola, T. Dyke, ibid, 72, 5062 (1980).

35. D. Hadzi, S. Bratos in "Vibrational Spectroscopy of the Hydrogen Bond," Chapter 12, Reference 11.

36. (a) See Reference 11, Ch. 6, "Dynamical Properties of Hydrogen Bonded Systems," G. C. Hofacker, Y. Marechal, and M. A. Ratner.
(b) Y. Marechal, A. Witkowski, J. Chem. Phys. 48, 3697 (1968).
(c) M. Wôjcik, Mol. Phys. 36, 1757 (1978).

37. M. Sceats, M. Stavola, S. Rice, J. Chem. Phys. 71, 983 (1979).

38. (a) Y. Bouteiller, Y. Guissani, Mol. Phys. 38, 617 (1979).

(b) J. Lascombe, J. C. Lassegues, Mol. Phys. 40, 969 (1980).

39. Reference 35, page 575.

40. "Infrared Fundamental Region," W. Luck in Structure of Water and Aqueous Solutions, W. A. P. Luck, ed., Verlag Chemie, Weinheim 1974.

41. (a) W. A. Senior, R. E. Verrall, J. Phys. Chem. 73, 4242 (1969).

(b) G. Walrafen, J. Chem. Phys. 114 (1967).

42. M. Sceats, K. Belsley, Mol. Phys. 40, 1389 (1980).

43. N. Koroteev, M. Endemann, R. Byer, Phys. Rev. Lett. 43, 398 (1979).

44. (a) A. Tursi, E. Nixon, J. Chem. Phys. 52, 152 (1970).

(b) L. Fredin, B. Nelander, G. Ribbegard, Chem. Phys. Lett. 36, 375 (1975).

(c) L. Fredin, B. Nelander, G. Ribbegard, J. Chem. Phys. 66, 4065 (1977), 4073 (1977).

(d) G. Ayers, A. Pullin, Spectra. Acta. 32A, 1689 (1976), 1695 (1976).

(e) R. M. Bentwood, A. J. Barnes, W. J. Orville-Thomas, J. Mol. Spectro. 84, 391 (1980).

(f) P. V. Hong, J. C. Cornut, J. Chim. Phys. 72, 534 (1975).

(g) D. Strommen, D. Gruen, R. McBeth, J. Chem. Phys. 58, 4028 (1973).

(h) H. Hallam, "Infrared Matrix Isolation Studies of Water, Ref. 40.

45. G. Girardet, D. Robert, J. Chem. Phys. 59, 5020 (1973).

46. J. E. Bertie, E. Whalley, ibid, 40, 1637 (1964).

47. J. E. Bertie, E. Whalley, ibid, 40, 1646 (1964).

48. (a) I. R. McDonald and M. L. Klein, ibid, 68, 4875 (1978).

(b) R. W. Impey, M. L. Klein, I. R. McDonald, ibid, J. Chem. Phys. 74, 647 (1981).

49. (a) R. O. Watts, Chem. Phys. 57, 185 (1981).

(b) R. O. Watts, Mol. Phys. 28, 1069 (1974).

(c) J. A. Barker, R. O. Watts, Chem. Phys. Lett. 3, 144 (1969).

(d) J. A. Barker, R. O. Watts, Mol. Phys. 26, 789 (1973).

(e) D. T. Evans, R. O. Watts, Mol. Phys. 28, 1233 (1974).

50. G. C. Lie, E. Clementi, J. Chem. Phys. 64, 5308 (1976).

51. (a) A. Rahman, F. H. Stillinger, H. L. Lemberg, ibid, 63, 5223 (1975).

(b) F. H. Stillinger, A. Rahman, ibid, 60, 1545 (1974).

(c) F. H. Stillinger, A. Rahman, ibid, 57, 1281 (1972).

(d) F. H. Stillinger, A. Rahman, ibid, 55, 3336 (1971).

52. M. Mezei, D. Beveridge, ibid, 74, 622 (1981).

53. W. Jorgensen, Chem. Phys. Lett. 70, 326 (1980).

54. F. Abraham, J. Chem. Phys. 61, 1221 (1974).

55. C. Briant, J. Burton, ibid, 63, 3327 (1975).

56. A. C. Belch, S. A. Rice, M. G. Sceats, Chem. Phys. Lett. 77, 455 (1981).

57. G. N. Sorkisov, V. G. Dashevsky, G. G. Malenkov, Mol. Phys. 27, 1249 (1974).

58. J. M. Lisy, M. F. Vernon, unpublished results.

59. (a) M. Sceats, S. A. Rice, J. Chem. Phys. 71, 973 (1979).

(b) M. Sceats, S. A. Rice, ibid, 71, 983 (1979).

(c) M. Sceats, S. A. Rice, ibid, 72, 3236 (1980).

60. P. Berens, K. Wilson, ibid, 74, 4872 (1981).

61. G. Herzberg, Molecular Spectra and Molecular Structure III, p. 585, Van Nostrand Reinhold Co. (1966).

62. CLAMPS--Classical Many Particle Simulator, Author-D. Ceperley, NRCC, 1979.

63. GRAMPS--Graphics language for use with Evans and Sutherland multipicture system, Author-T. J. O'Donnell, NRCC (1980).

64. J. M. Lisy, A. Tramer, M. F. Vernon and Y. T. Lee, J. Chem. Phys. 75, 4733 (1981).

65. J. B. Hopkins, D. E. Powers, and R. E. Smalley, "Mass Selective Two-Color Photoionization of Benzene Clusters," submitted to J. Phys. Chem.

66. P. R. R. Langridge-Smith, D. V. Brumbaugh, C. A. Haynam, D. H. Levy, "The Ultraviolet Spectra of Benzene Clusters," J. Phys. Chem. (submitted).

Table 1. Experimental conditions used to measure the vibrational predissociation spectra in Fig. 3. In all cases the angle between the detector and the molecular beam was 4°, and the nozzle temperature was 125°C.

Temperature of water reservoir	Pressure at nozzle (torr)	Ion mass detected	Fig. 3 label	Smallest water cluster capable of contribution to signal
67.5	209	H_3O^+	a	trimer
72	255	$(H_2O)_2\ H^+$	b	tetramer
80	355	$(H_2O)_3\ H^+$	c	pentamer
84	417	$(H_2O)_4\ H^+$	d	hexamer

Table 2. Water polymer energetics.

$D_e(cm^{-1})$	Fig. 5 Label	Watts	Owicki	Stillinger (C.F.)	Stillinger (Pol.)
H_2O		0.0	0.0	0.0	0.0
$(H_2O)_2$	a	2122.0	1904.0	1993.0	2388.0
$(H_2O)_3$	b	5450.0	5183.0	5472.0	3774.0
$(H_2O)_3$	c	--	--	--	5387.0
$(H_2O)_4$	d	9187.0	8624.0	7667.0	10147.0
$(H_2O)_4$	e	7526.0	--	--	--
$(H_2O)_5$	f	12100.0	12429.0	11980.0	15789.0

Harmonic ZPE (cm^{-1})	Fig. 5 Label	Watts	Owicki*	Stillinger (C.F.)	Stillinger (Pol.)
(H_2O)		4723.0	0.0	4739.0	5107.0
$(H_2O)_2$	a	10224.0	854.0	10320.0	11863.0
$(H_2O)_3$	b	16088.0	1876.0	18417.0	18870.0
$(H_2O)_3$	c	--	--	--	18597.0
$(H_2O)_4$	d	21682.0	3094.0	23897.0	26611.0
$(H_2O)_4$	e	21406.0	--	--	--
$(H_2O)_5$	f	27145.0	3941.0	28891.0	36252.0

Table 2. (continued).

$D_o(cm^{-1})$	Type	Fig. 5 Label	Watts	Owicki	Stillinger (C.F.)	Stillinger (Pol.)
(H_2O)			0.0	0.0	0.0	0.0
$(H_2O)_2$		a	1343.0	1050.0	1151.0	739.0
$(H_2O)_3$	MD	b	2187.0	2257.0	121.0	-514.0
$(H_2O)_3$	CD	b	3530.0	3307.0	1272.0	225.0
$(H_2O)_3$	MD	c	--	--	--	1072.0
$(H_2O)_3$	CD	c	--	--	--	2111.0
$(H_2O)_4$	MD	d	2866.0	2223.0	1454.0	1853.0
$(H_2O)_4$	CD	d	3709.0	3430.0	424.0	2486.0
$(H_2O)_4$	MD	e	1481.0	--	--	--
$(H_2O)_4$	CD	e	2324.0	--	--	--
$(H_2O)_5$	MD	f	2177.0	2958.0	4058.0	1108.0
$(H_2O)_5$	CD	f	3695.0	4131.0	4361.0	2222.0

*Rigid H_2O molecule. ZPE's of $(H_2O)_n$ are only from the motions associated with hydrogen bonding.

Table 3. Pressure dependence of the water cluster distribution in the molecular beam.

Pressure at Nozzle (Torr)	$\frac{(H_2O)_2\ H^+}{H_3O^+}$	$\frac{(H_2O)_3\ H^+}{H_3O^+}$	$\frac{(H_2O)_4\ H^+}{H_3O^+}$
150	0.19	0.02	---
185	0.34	0.10	0.02
235	0.54	0.25	0.08
290	0.66	0.43	0.17
355	0.78	0.46	0.32
435	0.92	0.68	0.48
525	1.0	0.75	0.57

Table 4. High frequency vibrations for potential models. The values in parentheses are the integrated band intensities (using a linear approximation to the dipole moment function) for the normal coordinates, normalized to the most intense free OH transition.

	Watts		Stillinger Central Force		Stillinger Polarization	
Monomer	3951(1.00)	1653(0.99)	4283(0.34)	1375(1.20)	4354(0.82)	1642(5.29)
	3841(0.52)		3820(1.00)		4203(1.00)	
	Fig. 5(a)		Fig. 5(a)		Fig. 5(a)	
Dimer	3920.(1.00)	1708.(0.90)	4363.(0.95)	1495.(3.09)	4689.(0.25)	1811.(0.25)
	3914.(0.87)	1670.(1.12)	4303.(1.00)	1415.(3.53)	4485.(1.00)	1638.(0.32)
	3815.(0.45)		3877.(2.68)		4455.(0.25)	
	3760.(0.73)		3834.(2.74)		4157.(0.28)	

	Fig. 5(b)		Fig. 5(b)		Fig. 5(b)		Fig. 5(c)	
Trimer	3890.(0.00)	1773.(0.00)	4545.(1.00)	2918.(0.00)	4680.(0.99)	1780.(0.03)	4848.(0.22)	1840.(0.13)
	3884.(1.00)	1727.(0.85)	4545.(1.00)	1840.(0.31)	4657.(1.00)	1703.(0.46)	4657.(0.22)	1816.(0.06)
	3884.(1.00)	1727.(0.85)	4422.(0.0)	1840.(0.31)	4464.(0.06)	1647.(0.39)	4517.(1.00)	1629.(0.14)
	3696.(0.80)		3959.(2.05)		4415.(0.11)		4496.(0.13)	
	3969.(0.80)		3959.(2.05)		4375.(0.53)		4412.(0.27)	
	3660.(0.00)		3894.(0.0)		4337.(0.75)		4138.(0.15)	

Table 4. Continued.

	Watts				Stillinger Central Force		Stillinger Polarization	
	Fig. 5(d)		Fig. 5(e)		Fig. 5(d)		Fig. 5(d)	
Tetramer	3888.(0.00)	1749.(0.00)	3924.(0.90)	1791.(0.17)	4677.(0.59)	2269.(1.44)	4864.(0.02)	1858.(0.06)
	3884.(1.00)	1733.(1.16)	3892.(0.47)	1748.(1.14)	4636.(0.65)	2138.(1.69)	4766.(1.0)	1772.(0.08)
	3884.(1.00)	1733.(1.16)	3886.(1.00)	1727.(1.27)	4461.(0.81)	1579.(1.12)	4766.(1.0)	1770.(0.08)
	3883.(0.00)	1733.(0.00)	3819.(0.27)	1669.(0.99)	4403.(1.00)	1548.(4.96)	4507.(0.0)	1770.(0.0)
	3741.(0.00)		3779.(1.01)		3994.(1.59)		4483.(0.0)	
	3727.(0.76)		3701.(0.95)		3982.(1.200)		4409.(0.48)	
	3727.(0.76)		3687.(0.69)		3949.(1.29)		4409.(0.48)	
	3704.(0.00)		3653.(0.12)		3911.(1.32)		4384.(0.18)	
	Fig. 5(f)				Fig. 5(f)		Fig. 5(f)	
Pentamer	3886.(0.02)	1737.(0.10)			4512.(0.0)	1652.(0.13)	4812.(0.12)	2173.(0.00)
	3882.(0.98)	1736.(0.27)			4506.(0.0)	1629.(2.92)	4747.(0.29)	2068.(0.08)
	3882.(1.00)	1736.(0.01)			4463.(1.00)	1627.(2.78)	4672.(1.00)	2059.(0.04)
	3881.(0.10)	1732.(1.31)			4463.(1.00)	1611.(0.14)	4663.(0.77)	2051.(0.04)
	3880.(0.26)	1731.(1.02)			4431.(0.0)	1606.(0.05)	4612.(0.28)	2001.(0.01)
	3744.(0.00)				3959.(1.61)		4408.(1.08)	
	3743.(0.00)				3957.(1.70)		4325.(0.42)	
	3729.(0.91)				3943.(2.14)		4272.(5.99)	
	3728.(0.91)				3943.(2.14)		4248.(7.40)	
	3713.(0.00)				3934.(0.0)		3985.(0.32)	

Table 5. Dipole moments of clusters for the minimum energy configurations characterizing the different potential models.

Cluster	Fig. 5 Label	Dipole Moments (Debye)		
		Watts	Polarization	Central Force
(H_2O)		1.85	1.854	1.85
$(H_2O)_2$	(a)	3.14	3.98	3.13
$(H_2O)_3$	(b)	0.00	1.16	----
$(H_2O)_3$	(c)	----	5.81	----
$(H_2O)_4$	(d)	0.00	0.00	0.83
$(H_2O)_4$	(e)	1.97	----	----
$(H_2O)_5$	(f)	0.15	1.04	0.06

Table 6. Comparison of assigned matrix $(H_2O)_2$ transitions with the Watts potential model.

Watts' Harmonic Frequencies	Watts' Scaled Frequencies	Ar Matrix	Diff.	Watts' Scaled to Ar	Diff.
	(X.951)			(X.950)	
3920.	3729.	3726.	+3	3724	+2
3914.	3723.	3709.	+14	3718	+9
3815.	3629.	3634.	-5	3624	-10
3760.	3577.	3574.	+3	3572	-2
		N_2 Matrix		Watts' Scaled to N_2 (X.947)	
		3715	+19	3712	-3
		3699	+24	3707	+8
		3627	+2	3613	-14
		3550	+22	3561	+11

Figure Captions

Fig. 1. In plane view of perpendicular laser molecular beam apparatus. Labeled components are: 1) 0.007 in. diameter quartz nozzle heated to 125°C, 2) first skimmer, 3) second skimmer, 4) third skimmer, 5) power meter, 6) Germanium filter, 7) ionizer assembly, 8) quadrupole mass spectrometer. ⊖ measures the angle of rotation of the detector from the molecular beam.

Fig. 2. Schematic diagram of the Nd:YAG pumped OPO. Components indicated are: 1) Telescope, 2) input coupler (100 percent transmittance at 1.06μ, 100 percent reflectance at 1.4–2.1μ), 3) gold mirror, 4) 30°C temperature stabilized, angle tuned $LiNbO_3$ crystal, 5) output coupler (100 percent transmittance at 1.06μ, 50 percent reflectance at 1.4–2.1μ), 6) double pass YAG mirror (100 percent reflectance at 1.06μ, 100 percent transmittance at 1.4–4.0μ), 7) BaF_2 lens.

Fig. 3. Water cluster and condensed phase spectra. Panels (a)-(d) are spectra observed in the present work for the conditions given in Table I. Panel (e) conditions are described in the text. Panel (f) is taken from Ref. 9, Panel (g) from Ref. (14b), Panel (h) from E. Whalley and J. E. Bertie, J. Chem. Phys. 46, 1264 (1967).

Fig. 4. Laboratory angular distributions for the detected mass ○ - H_2O^+; + - $(H_2O)_2\ H^+$; □ - $(H_2O)_3\ H^+$; ● - $(H_2O)_4\ H^+$.

Fig. 5. Minimum energy cluster geometries for the Watts potential energy function (a,b,d,e,f), for the polarization model trimer (c), and for the configuration characterizing a transition state for the tetramer dissociating into a trimer and a monomer (g).

Fig. 6. Schematic representation of a hypothetical intermolecular charge transfer cluster configuration.

Fig. 7. Locally adiabatic dissociation energy curves for A. $(H_2O)_2 \rightarrow 2H_2O$, B. $(H_2O)_3 \rightarrow (H_2O)_2 + H_2O$, C. $(H_2O)_4 \rightarrow (H_2O)_3 + H_2O$ when adjacent hydrogen bonded waters are separated, D. $(H_2O_4 \leftarrow (H_2O)_3 + H_2O$ when it is formed from a monomer adding to a cyclic trimer, E. $(H_2O)_4 \rightarrow (H_2O)_3 + H_2O$ when opposing nonhydrogen bonded water molecules of the cyclic tetramer are separated.

Fig. 8. The decay curves of the molecular dynamics trajectories for the conditions

- ● $T_{vib} = 3000^\circ K$, $T_{rot} = 0^\circ K$
- \+ $T_{vib} = 3000^\circ K$, $T_{rot} = 100^\circ K$
- □ $T_{vib} = 3000^\circ K$, $T_{rot} = 200^\circ K$
- ○ $T_{vib} = 5000^\circ K$, $T_{rot} = 100^\circ K$

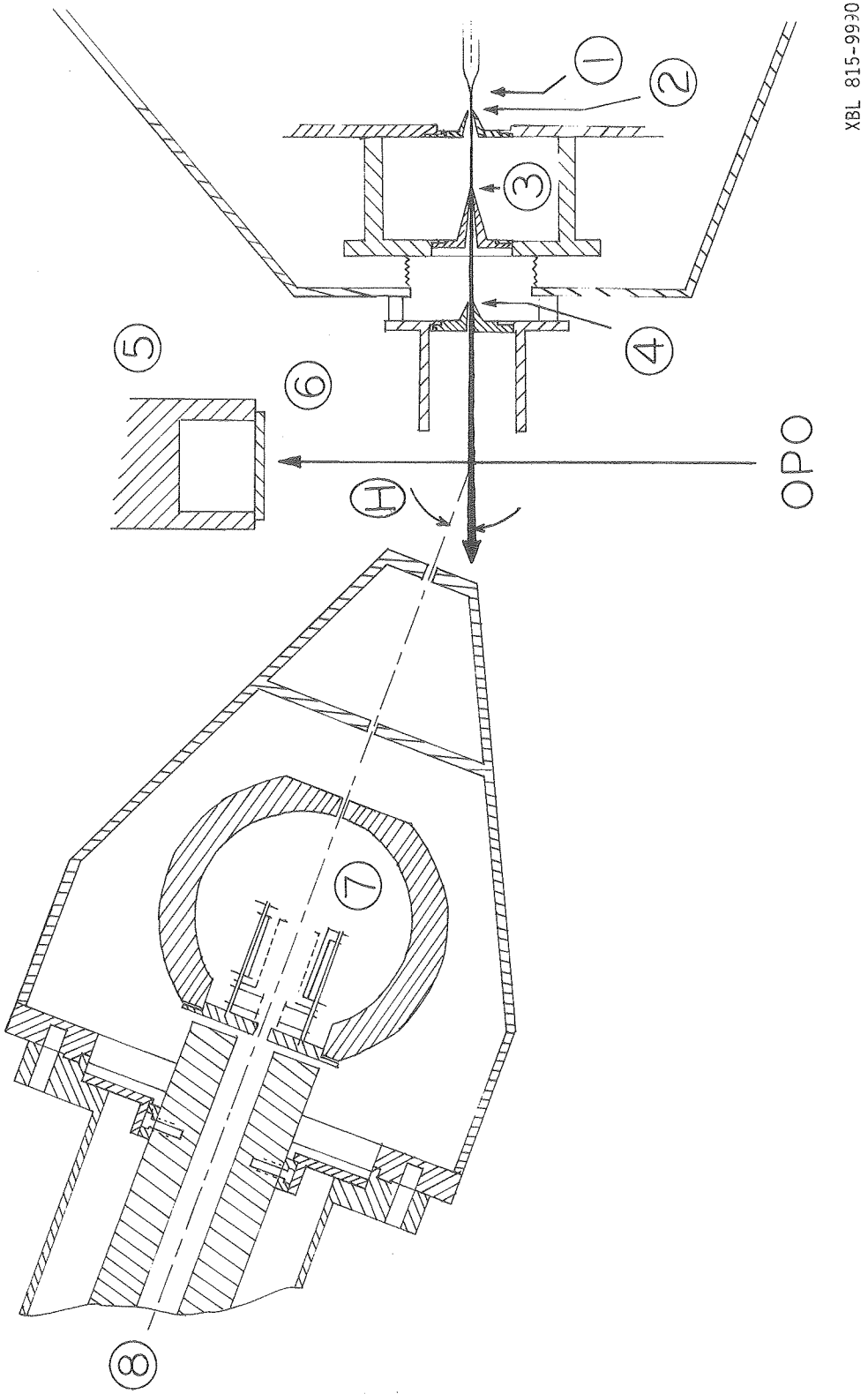

XBL 815-9930

Fig. 1

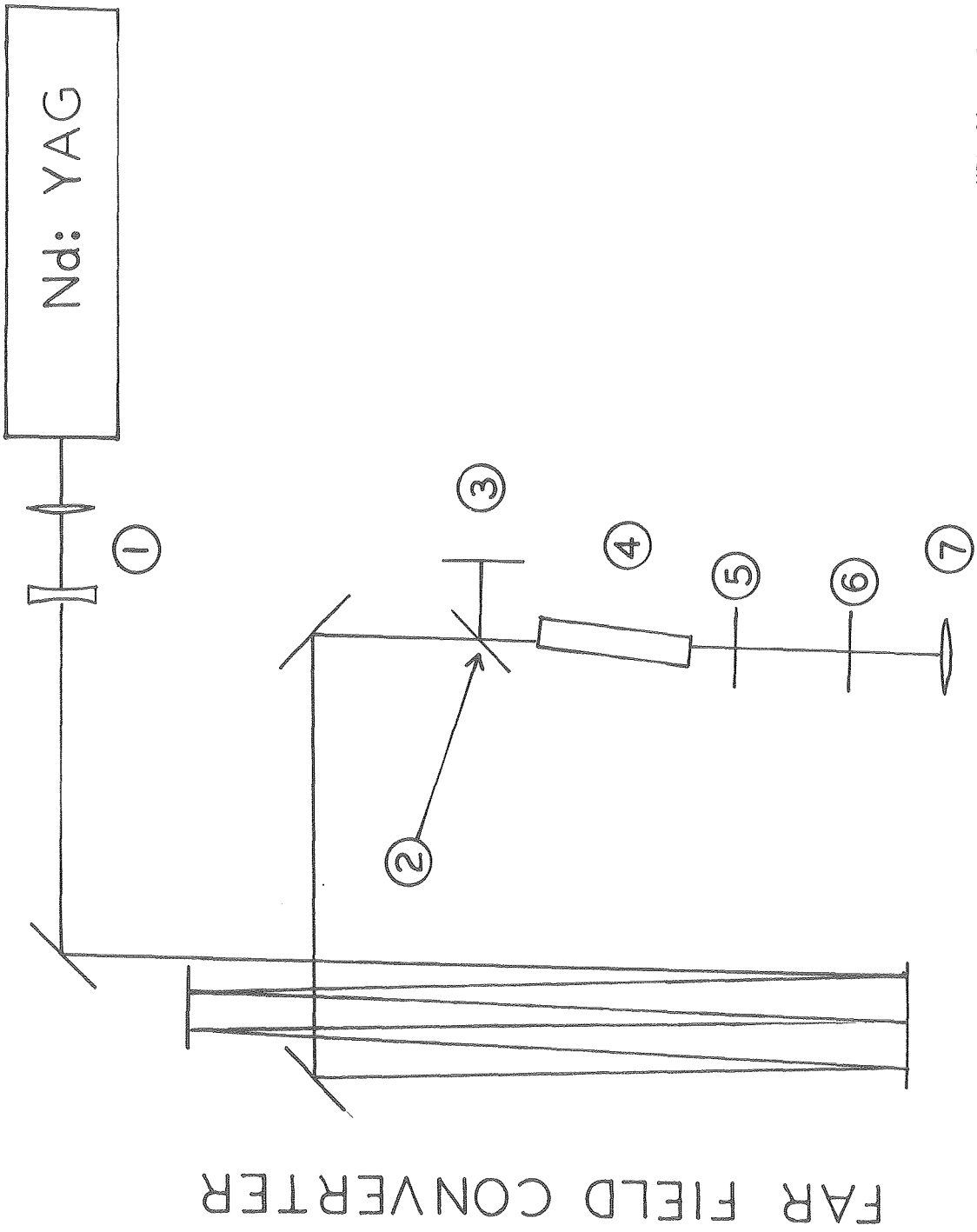

XBL 815-9991

Fig. 2

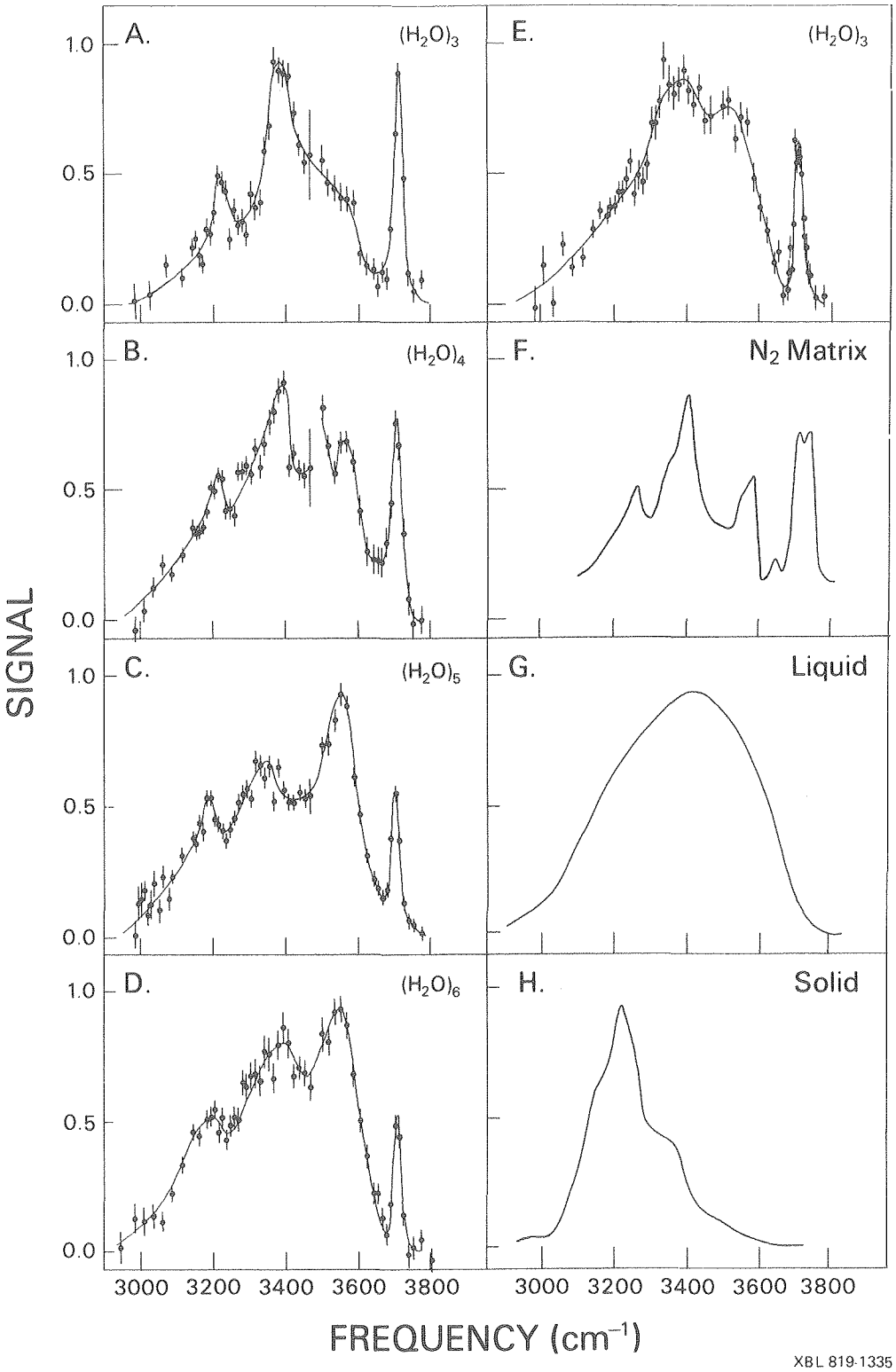
A.
$(H_2O)_3$
B.
$(H_2O)_4$
C.
$(H_2O)_5$
D.
$(H_2O)_6$
E.
$(H_2O)_3$
F.
N_2 Matrix
G.
Liquid
H.
Solid
SIGNAL
1.0
0.5
0.0
3000 3200 3400 3600 3800
FREQUENCY (cm^{-1})
XBL 819-1335

Fig. 3

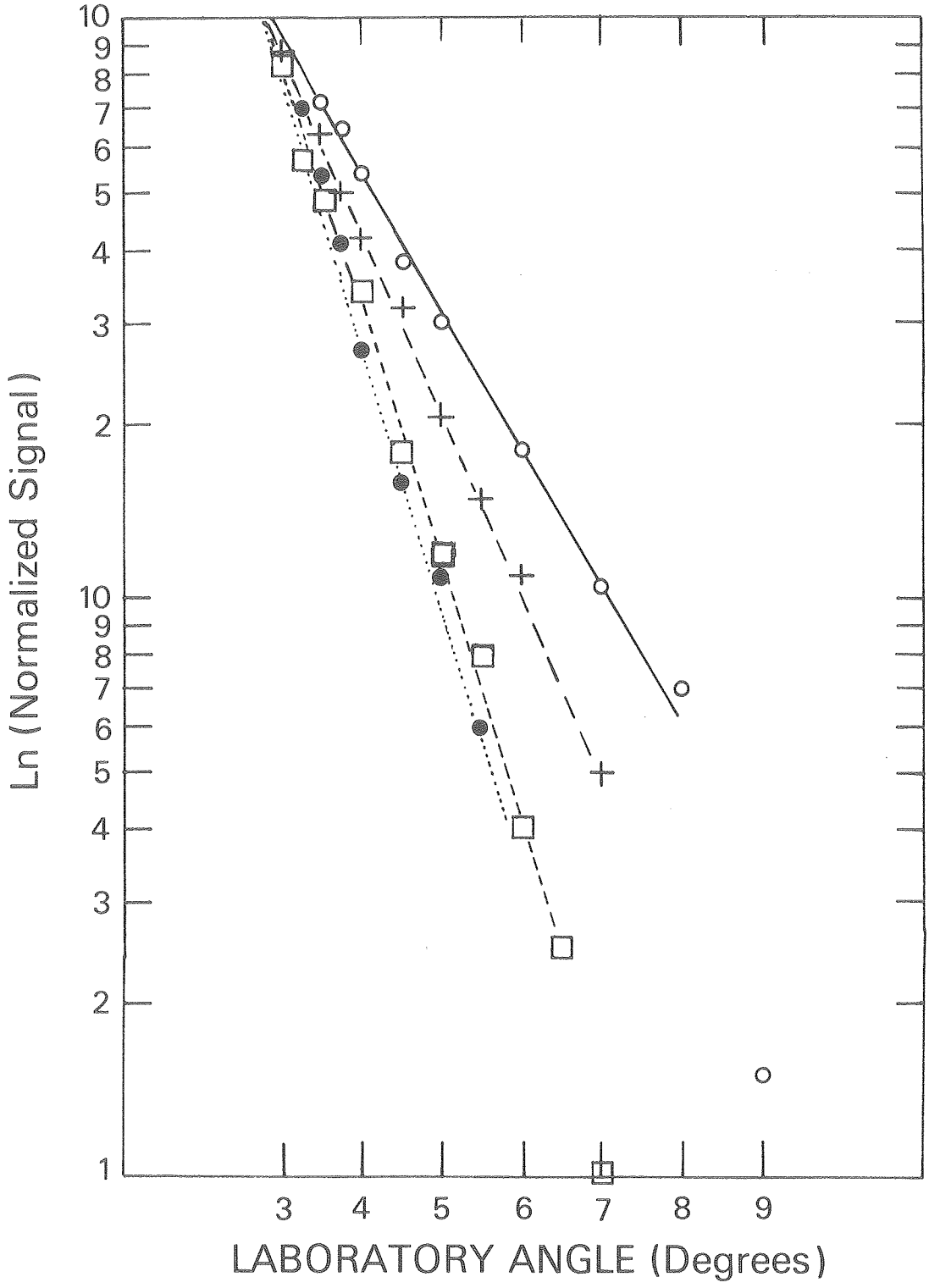

XBL 819-1333

Fig. 4

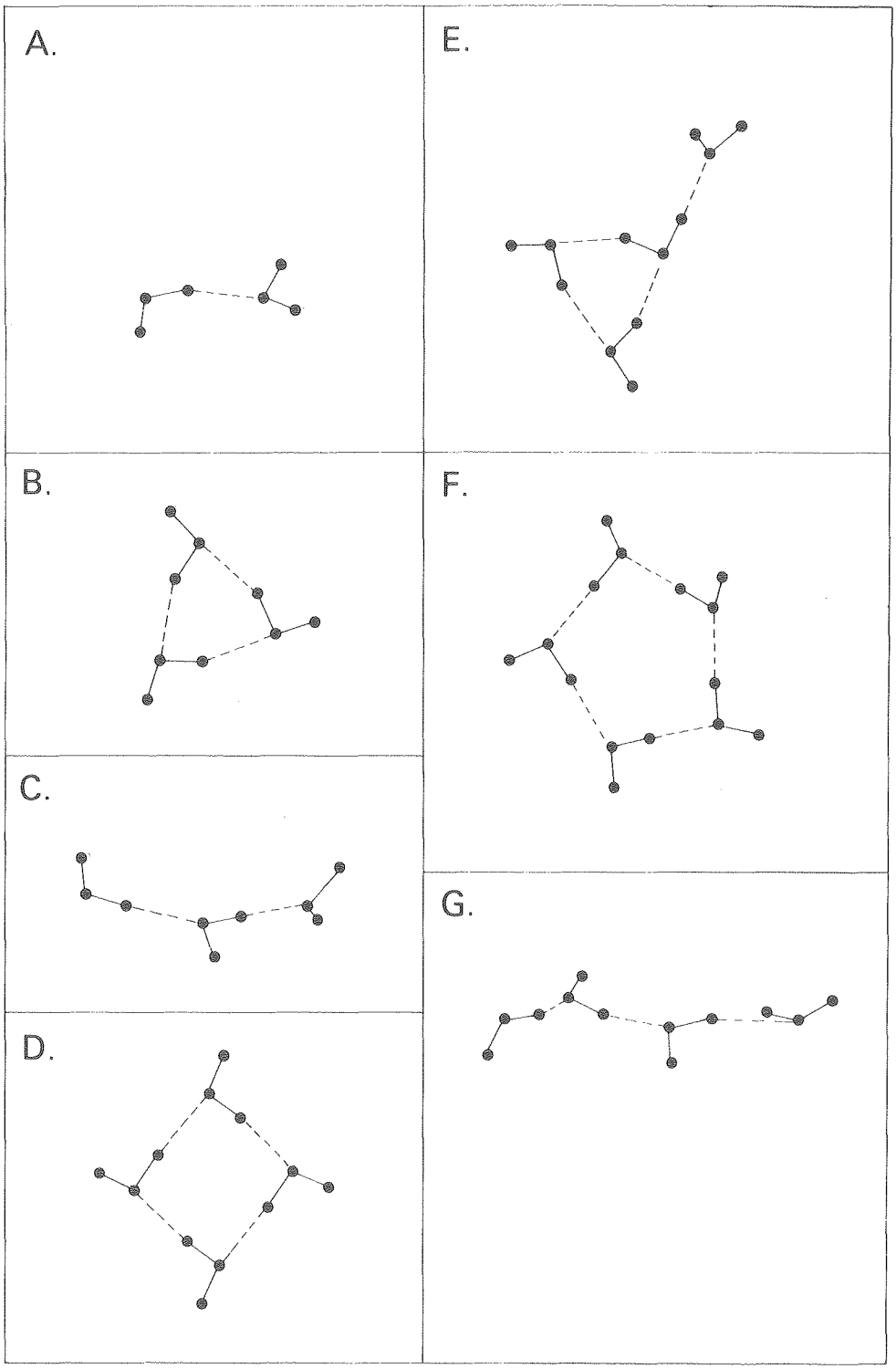

XBL 819-1334

Fig. 5

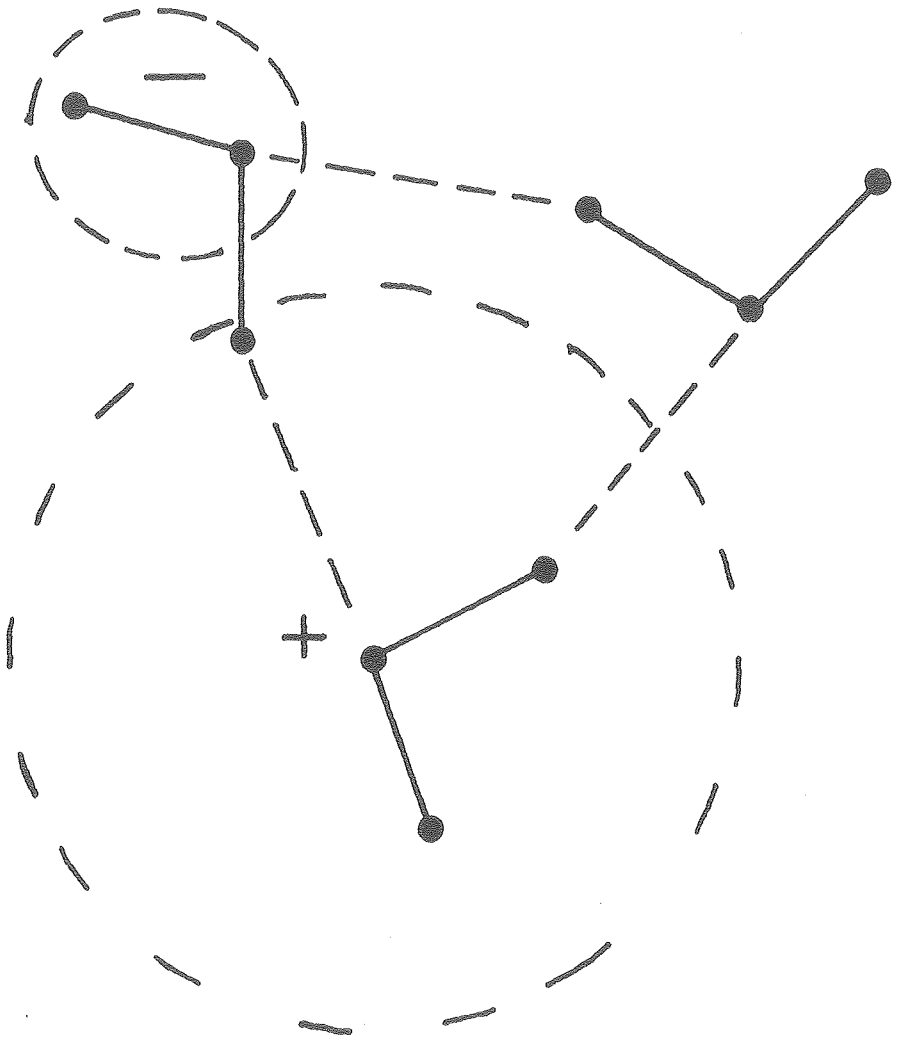

XBL 819-4968

Fig. 6

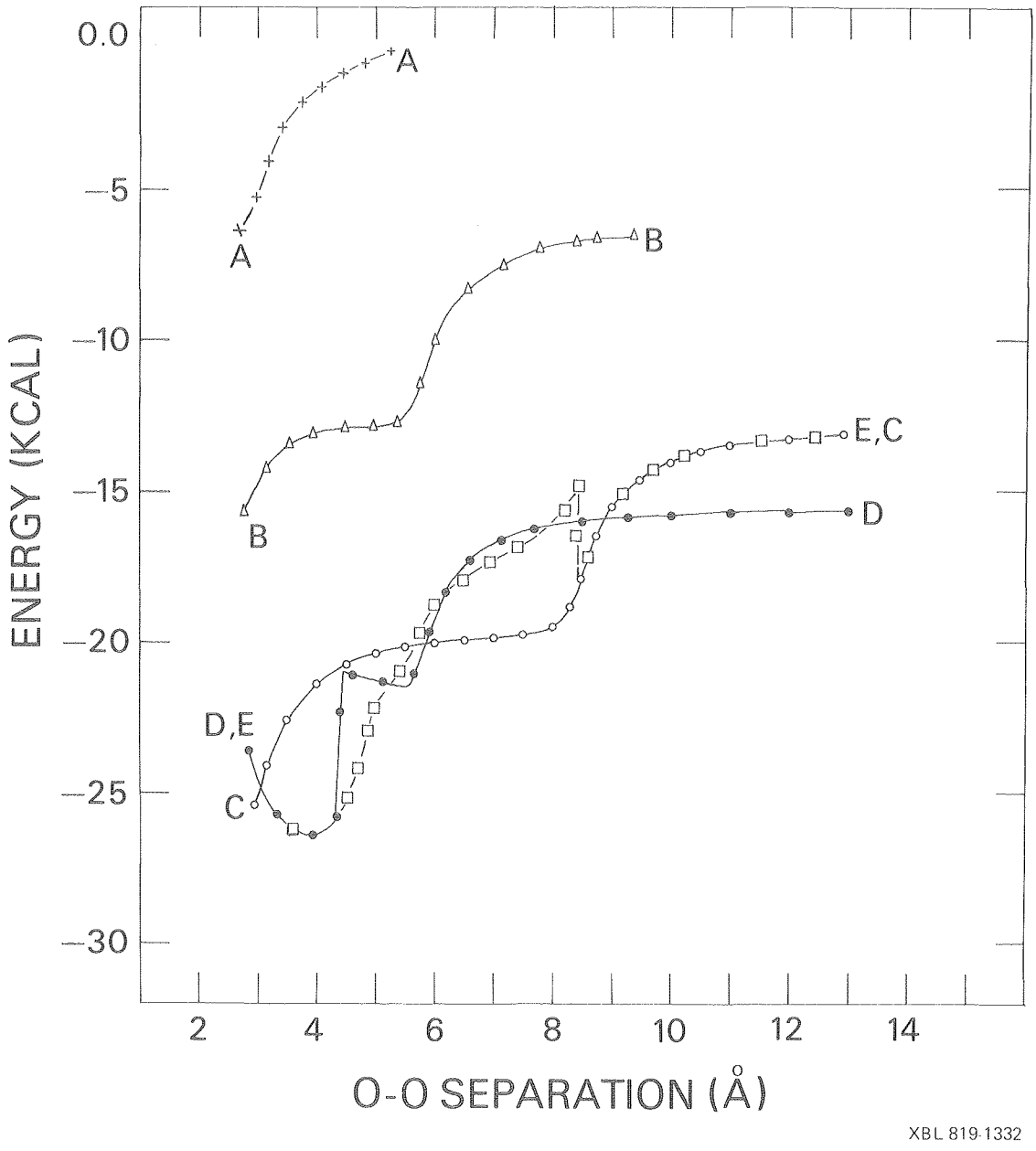
0.0
−5
−10
−15
−20
−25
−30
ENERGY (KCAL)
2
4
6
8
10
12
14
O-O SEPARATION (Å)
A
A
B
B
E,C
D
D,E
C
XBL 819-1332

Fig. 7

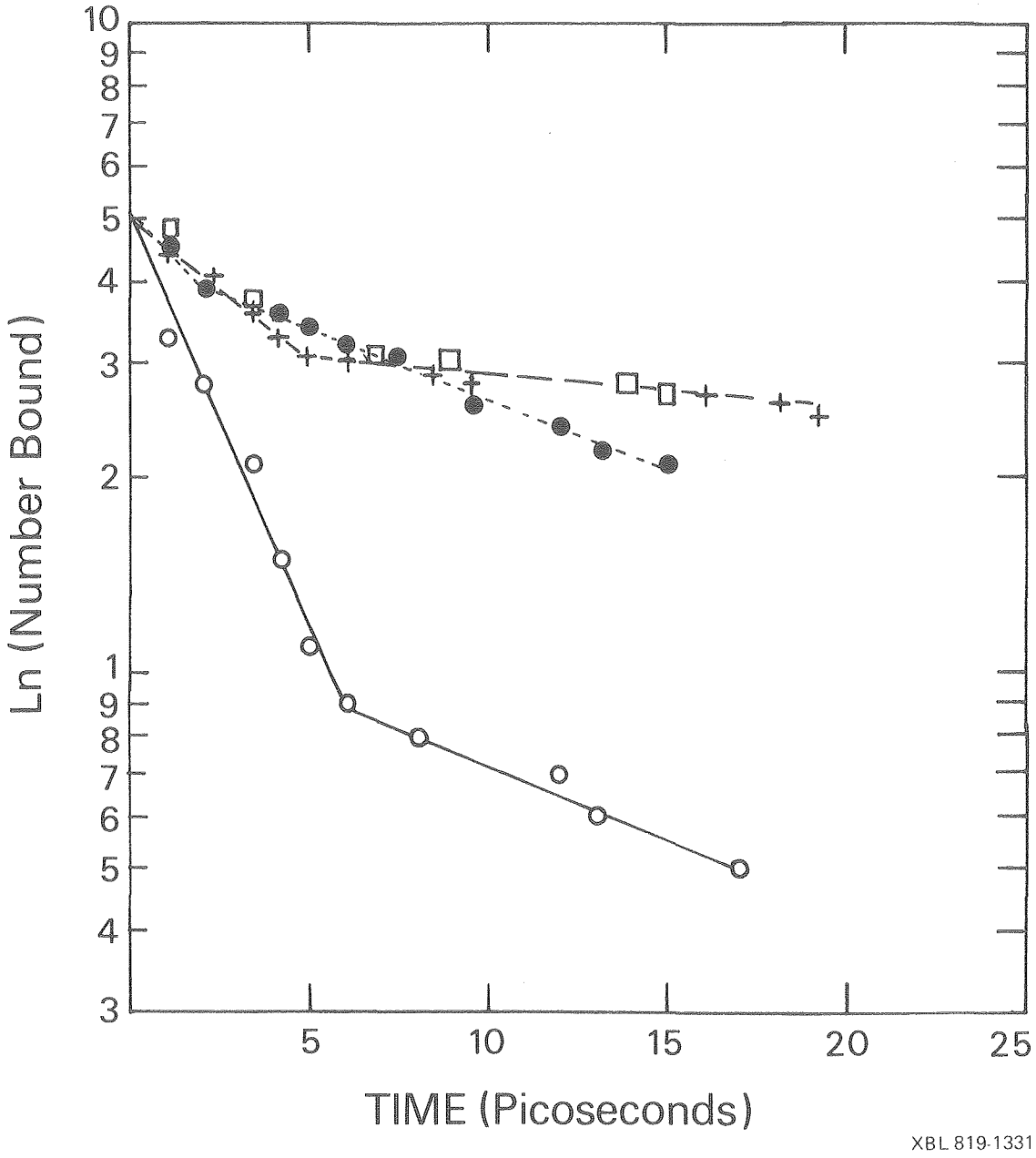
Ln (Number Bound)
10
9
8
7
6
5
4
3
2
1
9
8
7
6
5
4
3
5
10
15
20
25
TIME (Picoseconds)
XBL 819-1331

Fig. 8